

Proceedings of

MMM ● ● ●
Third International Conference
Multiscale Materials Modeling
September 18-22, 2006, Freiburg, Germany

Symposium 8
Multiscale simulation
approaches for static and
dynamic properties of
macromolecular materials

Peter Gumbsch
Editor and Conference Chair

Organized by Fraunhofer-Institute for Mechanics of Materials.
Hosted by University of Freiburg.


Fraunhofer Institut
Werkstoffmechanik


ALBERT-LUDWIGS-
UNIVERSITÄT FREIBURG

Imprint

Papers published in this volume constitute the proceedings of the Third International Conference on Multiscale Materials Modeling. Papers were selected by the program committee for oral or poster presentation. They are published as submitted, in the interest of timely dissemination.

Contact
Fraunhofer Institute for Mechanics of Materials IWM
Woehlerstraße 11
79108 Freiburg
Germany
Phone + 49 761 5142 0
Fax + 49 761 5142 110

The complete proceedings of the conference are available at

Fraunhofer Information-Centre for Regional Planning and Building Construction IRB
P.O. Box 80 04 69, D-70504 Stuttgart
Nobelstrasse 12, D-70569 Stuttgart
Fon +49 (0) 7 11/9 70-25 00
Fax +49 (0) 7 11/9 70-25 07
E-Mail irb@irb.fraunhofer.de
URL www.irb.fraunhofer.de
ISBN-10: 3-8167-7206-4
ISBN-13: 978-3-8167-7206-4

Foreword

Computational modeling of materials behavior by multiscale materials modeling (MMM) approaches is becoming a reliable tool to underpin scientific investigations and to complement traditional theoretical and experimental approaches of component assessment. At transitional (microstructural) scales continuum approaches begin to break down and atomistic methods reach inherent limitations in time and length scale. Transitional theoretical frameworks and modeling techniques are developed to bridge the gap between the different length scales.

Industrial success in high technology fields relies on the possibility to specifically engineer materials and products with improved performance. The success factor is the ability to make these material related developments timely at relatively low-costs. This demands not only the rapid development of new or improved processing techniques but also better understanding and control of material chemistry, processing, structure, performance, durability, and their relationships. This scenario usually involves multiple length and time scales and multiple processing and performance stages, which are usually only accessible via multi-scale / multi-stage modeling or simulation.

In high-payoff, high-risk technologies such as the design of large structures in the aerospace and nuclear industries, the effects of aging and environment on failure mechanisms cannot be left to conservative approaches. Increasing efforts are now focused on advancing MMM approaches to develop new material systems components and devices. Appropriate validation experiments are crucial to verify that the models predict the correct behavior at each length scale. Thus, one of the advantages of these MMM approaches is that, at each scale, physically meaningful parameters are predicted and used in models for subsequent scales, avoiding the use of empiricism and fitting parameters.

Recent interest in nanotechnology is challenging the scientific community to design nanometer to micrometer size devices for applications in new generations of computers, electronics, photonics or drug delivery systems. These new application areas of multiscale materials modeling require novel and sophisticated science-based approaches for design and performance evaluation. Theory and modeling are playing an increasing role to reduce development costs and manufacturing times. With the sustained progress in computational power and MMM methodologies, new materials and new functionalities are increasingly more likely discovered by MMM approaches than by traditional trial and error approach. This is part of a paradigm shift in modeling, away from reproducing known properties of known materials towards simulating the behavior of hypothetical composites as a forerunner to finding real materials with these novel properties.

The MMM 2006 conference provides an international forum for the scientific advances of multiscale modeling methodologies and their applications.

I would like to thank the members of the international advisory committee, the local program committee and particularly the organizing team, the symposium organizers and the session chairs and the University of Freiburg for their engagement and support. Without their hard work and their devotion of time and resources, the Third International Conference Multiscale Materials Modeling would not have been possible.

Finally, I would like to thank our conference sponsors for their financial support: The German Research Foundation DFG, Accelrys Inc., Plansee S.E. and the Ministry of Science, Research and Art, Baden-Württemberg.

Peter Gumbsch
Conference Chair

Conference Committee

International Advisory Committee

Prof. Bacon, David	University of Liverpool, UK
Dr. Baskes, Michael	Los Alamos National Laboratory, USA
Prof. Busso, Esteban	Imperial College, London, UK
Prof. Cale, Timothy S.	Rensselaer Polytechnic Institute, Troy, USA
Dr. Diaz de la Rubia, Tomas	Lawrence Livermore National Lab., USA
Prof. Ghoniem, Nasr	University of California, Los Angeles, USA
Prof. Guo, Xiao	Queens College, London, UK
Prof. Iwata, Shuichi	University of Tokyo, Japan
Prof. Kratochvil, Jan	Technical University, Prague, Czech Republic
Prof. Kremer, Kurt	Max Planck Institute, Mainz, Germany
Dr. Kubin, Ladislav	ONERA-LEM, Chatillon, France
Dr. LeSar, Richard	Los Alamos National Laboratory, USA
Prof. Meguid, Shaker	University of Toronto, Canada
Prof. Needleman, Alan	Brown University, Providence, USA
Prof. Odette, Robert	University of California, Santa Barbara, USA
Prof. Ortiz, Michael	California Institute of Technology, USA
Prof. Pettifor, David	Oxford University, UK
Prof. Phillips, Robert	California Institute of Technology, USA
Prof. Raabe, Dierk	Max Planck Institute, Düsseldorf, Germany
Prof. Shibutani, Yoji	Osaka University, Japan
Dr. Soneda, Naoki	Komae Research Laboratory, Tokyo, Japan
Prof. Suresh, Subra	Massachusetts Institute of Technology, USA
Prof. Tomita, Yoshihiro	Kobe University, Japan
Prof. Van der Giessen, Erik	University of Groningen, Netherlands
Prof. Walgraef, Daniel	Free University of Brussels, Belgium
Dr. Wolf, Dieter	Argonne National Laboratory, USA
Prof. Yip, Sidney	Massachusetts Institute of Technology, USA
Dr. Zinkle, Steve	Oak Ridge National Laboratory, USA

Organizing Committee

M. J. Alava	Helsinki University of Technology, Finland
D. Dimiduk	The Ohio State University, USA
M. Dao	Massachusetts Institute of Technology, USA
M. Doi	University of Tokyo, Japan
C. Elsässer	Fraunhofer IWM, Germany
E. v. d. Giessen	University of Groningen, Netherlands
N. Gov	The Weizmann Institute of Science, Israel
H. J. Herrmann	University of Stuttgart, Germany
R. James	University of Minnesota, USA
K. Kremer	Max Planck Institute for Polymer Research, Germany
J. Korvink	IMTEK, University of Freiburg, Germany
J. Li	The Ohio State University, USA
S. Müller	Max Planck Institute for Mathematics in the Sciences, Germany
A. Paxton	Queen's University, Belfast, UK
M. Payne	University of Cambridge, UK
D. Raabe	Max Planck Institute fuer Eisenforschung, Germany
N. Soneda	Central Research Institute of Electric Power Industry, Japan
M. Zaiser	University of Edinburgh, UK
S. Zapperi	University of Rome, Italy
F. Willaime	Commissariat a l'Energie Atomique (CEA), France
B. Wirth	University of California, Berkeley, USA

Contents

Symposium 8

Dissipative Particle Dynamics Simulation for Formation Process of Threadlike Micelles under Shear Flow N. Arai, K. Yasuoka, Y. Masubuchi Session 8JM	913
Particle based modeling of ultrasonic plastification with a yield-stress fluid C. Bretthauer, D. Kauzlari, C. Müller, J. Korvink Session 8P	917
Computer Simulations of the Dynamics of Polymer Solutions B. Duenweg Session 8P	921
Atomistic, Mesoscale and Finite Element techniques for polymer materials simulations G. Goldbeck-Wood, J. Wescott, R. Akkermans, A. Maiti Session 8O	928
Hierarchical Material Simulation and Coarse Graining S. Hyodo Session 8N	932
Multiscale Equilibration of Poly (ethylene terephthalate) Melt K. Kamio, D. N. Theodorou, K. Moorthi Session 8O	935
Effects of hydrodynamic coherence on DNA translocation: a Lattice Boltzmann-Molecular Dynamics multiscale approach E. Kaxiras Session 8P	939
Statistics in entangled polymers from primitive chain network simulations Y. Masubuchi, G. Ianniruberto, F. Greco, G. Marrucci Session 8P	940
Challenges in Polymer Simulation F. Mueller-Plathe Session 8O	943
Modeling the polymer-precursor synthesis of the amorphous ceramic α -Si ₃ B ₃ N ₇ via a separation of time scale stepping stone approach C. Schoen, A. Hannemann, M. Jansen Session 8O	944
Hierarchical Modelling of Polymer Physical Properties D. N. Theodorou Session 8N	947
Mesoscopic Simulation of Micellar Structures in Amphiphilic Block Copolymer Solutions by the Density Functional Model T. Uneyama Session 8O	950
Modeling and simulation of dot formation kinetics in the drying process of polymer solution drop T. Yamaue, Y. Jung, M. Doi Session 8P	953

Symposium 8

**Multiscale simulation
approaches for static and
dynamic properties of
macromolecular materials**

Dissipative Particle Dynamics Simulation for Formation Process of Threadlike Micelles under Shear Flow

Noriyoshi Arai¹, Kenji Yasuoka¹ and Yuichi Masubuchi²

¹Department of Mechanical Engineering, Keio University, Yokohama 223-8522, Japan,
arai@a5.keio.jp, yasuoka@mech.keio.ac.jp

²Department of Organic and Polymer Materials Chemistry, Tokyo University of
Agriculture and Technology, Koganei, Tokyo 184-8588, Japan,
mas@rheo.chem.tuat.ac.jp

ABSTRACT

A micelle is the self-assembly of surfactant molecules formed in surfactant aqueous solution. The micelle has various forms such as a threadlike, spherical, discoid, and bilayer. Particularly, the threadlike micelle has the great possibility of the application in the industry, utilizing the uniqueness in its formation. However, an overall understanding of the formation dynamics of the threadlike micelle has not been accomplished, because of the so-called ‘mesoscopic problem’ in dynamics. In order to understand this phenomenon, the Molecular Dynamics (MD) method cannot be applied to this system, because the time scale and the length scale of this method are too short. And the Fluid Mechanics method cannot be applied to this system, too, because this method cannot be considered molecular structures. The aim of this study is to clarify the mesoscale dynamics of the threadlike micelles by means of the Dissipative Particle Dynamics (DPD) simulation. DPD method is a comparatively new simulation method proposed by Hoogerbrugge and Koelman in 1992 and can treat the mesoscale range of time and length scales by many orders of magnitude compared to MD simulation. Moreover, the shear stress was put on a similar system, and it compared it without shear stress.

1. Introduction

A surfactant is a molecule, which is composed of hydrophilic and hydrophobic parts, and it has two characteristic features in water. One is that it adsorbs on a vapor-liquid surface and the surface tension is decreased. Another is that it spontaneously aggregates to form a wide variety of assemblies in aqueous solution such as spherical micelles, threadlike micelles, and vesicles. Particularly, the threadlike micelles has been expected to apply to the cement[1], the drag reduction[2], etc.

We know that threadlike micellar solution shows the characteristic viscoelastic behavior, which is similar to that in semidilute and concentrated polymer systems because the micelles is very stable. On the other hand the relaxation of threadlike micellar solution was observed as a Maxwell-type relaxation with a single relaxation time as opposed to that of polymer systems[3-5]. That mean the relaxation time of the threadlike micelles is much shorter than that of the polymer. Based on the experimental results, Shikata *et al.* proposed *the phantom network model* to explain this relaxation behavior[4,5]. In this model, the threadlike micelles were not entangled and passed through each other. However, in the molecular point of view the breakage and reforming of the threadlike micelles may be considering during the process

of the crossing for the micelles. Yamamoto and Hyodo[6] recently studied the crossing dynamics using the dissipative particle dynamics (DPD) simulation which is one of the coarse-grained model simulations. They reported that there were three kinds of schemes in the crossing dynamics such as the phantom crossing, the cutdown and the breakdown, thereby the breakage which occurs at somewhere along the threadlike micelle was the essential process in the relaxation mechanism and the phantom crossing can be seen as a special case of these processes. In the previous studies what the breakage and reformatting are the important process were reported, but the formation process of the threadlike micelles was not known and a further investigation of this phenomena is needed. The formation process might make a contribution to the viscoelastic behavior. Moreover, the breakage and re-formation is frequently done in above-mentioned crossing mechanism, hence the understanding of the formation process of threadlike micelles is indispensable.

The purpose of this paper is to clarify formation dynamics of the threadlike micelles in mesoscopic range where global motion of surfactant molecules is in focus while atomic dynamics in the molecules is somehow neglected. DPD method[7] was employed with an earlier proposed surfactant model[6] which has been confirmed to reproduce a stable threadlike micellar structure.

In this study, it is emphasized that the formation process of the threadlike micelles was firstly observed. From the obtained time evolution of the system, we calculated the aggregation number, radius of a micelle, length of a micelle and the ratio of principal moments of inertia. Moreover, the shear stress was put on a similar system, and it compared it without shear stress.

2. Simulation Method

2.1 DPD Simulation

The dynamics of threadlike micelles is in the multi scale range of time and length scales. The “*micro scale dynamics*” of the threadlike micelles is the formation process of the micelles and the molecular motion in the threadlike micelles with the time scale on the order of ps to ns. The “*macro scale dynamics*” is entanglement and phantom crossing dynamics of the threadlike micelles with the time scale longer than 1 ms. Shikata and his coauthors reported that the “*micro scale dynamics*” for the cationic surfactant micelles are independent the “*macro scale dynamics*” and the “*micro scale dynamics*” for the nonionic surfactant micelles are dependent on the “*macro scale dynamics*”[5]. However, the meso scale dynamics of the threadlike micelles, which are the formation process, are incompletely understood because this scale is too short in the experiment and too long in the Molecular Dynamics (MD).

DPD method[7] is a comparatively new calculation method constructed to base on the fluctuation-dissipation theorem by Hoogerbrugge and Koelman in 1992. This method based on Newton's equation of motion. The force is a total of a conservative force(F_{ij}^C), a pairwise random force(F_{ij}^R) and a dissipative force(F_{ij}^D).

$$m \frac{d\mathbf{v}_i}{dt} = \mathbf{f}_i = \sum_{j \neq i} F_{ij}^C + \sum_{j \neq i} F_{ij}^R + \sum_{j \neq i} F_{ij}^D \quad (1)$$

The conservative force is a soft repulsion acting on particles and is given by

$$\sum_{j \neq i} F_{ij}^C = \begin{cases} -a_{ij} \left(1 - \frac{|\mathbf{r}_{ij}|}{r_c} \right) \mathbf{n}_{ij}, & |\mathbf{r}_{ij}| \leq r_c \\ 0, & |\mathbf{r}_{ij}| > r_c \end{cases} \quad (2)$$

where, a_{ij} is the maximum repulsion between particles i and j , r_c is a cutoff distance, $\mathbf{r}_{ij} = \mathbf{r}_i - \mathbf{r}_j$, and $\mathbf{n}_{ij} = \mathbf{r}_{ij} / |\mathbf{r}_{ij}|$. A random force and dissipative force are given by

$$\sum_{j \neq i} F_{ij}^R = \begin{cases} \sigma \omega^R(\mathbf{r}_{ij}) \zeta_{ij} \Delta t^{-1/2} \mathbf{n}_{ij}, & |\mathbf{r}_{ij}| \leq r_c \\ 0, & |\mathbf{r}_{ij}| > r_c \end{cases}, \quad \sum_{j \neq i} F_{ij}^D = \begin{cases} -\gamma \omega^D(\mathbf{r}_{ij}) (\mathbf{n}_{ij} \cdot \mathbf{v}_{ij}) \mathbf{n}_{ij}, & |\mathbf{r}_{ij}| \leq r_c \\ 0, & |\mathbf{r}_{ij}| > r_c \end{cases} \quad (3)$$

respectively, σ is a noise parameter, γ is a friction parameter, ω^R and ω^D are \mathbf{r} -dependent weight functions, $\mathbf{v}_{ij} = \mathbf{v}_i - \mathbf{v}_j$ and ζ_{ij} is a randomly fluctuating variable with Gaussian statistics. Espan˜ol and Warren showed that one of the two weight functions appearing in Eqn. (3) can be chosen arbitrarily[8]. There is also a relation between the amplitudes and $k_B T$. In summary

$$\omega^D(r) = [\omega^R(r)]^2 = \begin{cases} 1 - \frac{r}{r_c}, & r \leq r_c \\ 0, & r > r_c \end{cases}, \quad \sigma^2 = 2\gamma k_B T \quad (4)$$

where k_B is a Boltzmann constant and T is a temperature. Eqn. (4) is a fluctuation-dissipation theorem.

In this study, we employed a spring force (F_{ij}^S), because the surfactant is considered as a harmonic spring for the equilibrium bond distance r_s

$$F_{ij}^S = -C \left(1 - \frac{|\mathbf{r}_{ij}|}{r_s} \right) \mathbf{n}_{ij} \quad (5)$$

where C is a spring constant.

The advantage of the DPD method is to be able to put it in easily after the model of a complex fluid element.

2.2 Simulation Conditions

In this study, we decided the parameters referring to early studies of Yamamoto and Hyodo[6]. The surfactant is composed of three particles. One of them is hydrophilic group(h). The others are hydrophobic group(t_1 , t_2). And we considered that water is one particle(w). The Interaction of each particle is equation (1).

Total number of particle in our simulation is 135,000 at a particle density ρ of 5. Among 4,725 particles are surfactant molecules, and the others are water molecules. As the initial configuration, all of particles were located randomly. In the DPD simulation, it is general to make various physical quantities dimensionless. In this study, the units of mass, length, and energy are chosen by the particle mass m , the cutoff distance r_c and the temperature $k_B T$, respectively. Also the spring constant is set at 100 and the bond distance is set at 0.86. The noise parameter σ is set at 3.0 and the friction parameter γ is set at 4.5. The simulation box

is set to cubic. The dimensionless length of the box is 30^3 . We used a periodic boundary condition, and Lees-Edwards boundary condition in shear flow.

3. Results

The major finding is that there are two stages in the formation process of threadlike micelles (Fig. 1). In the first stage, randomly dispersed surfactant molecules aggregated into several isolated spherical micelles in a short period corresponding to the diffusion time of the surfactant molecule up to 120 molecules per micelle. In the second stage, the spherical micelles, which were formed in the first stage, gradually connected each other and grew up to a rodlike and threadlike shape.

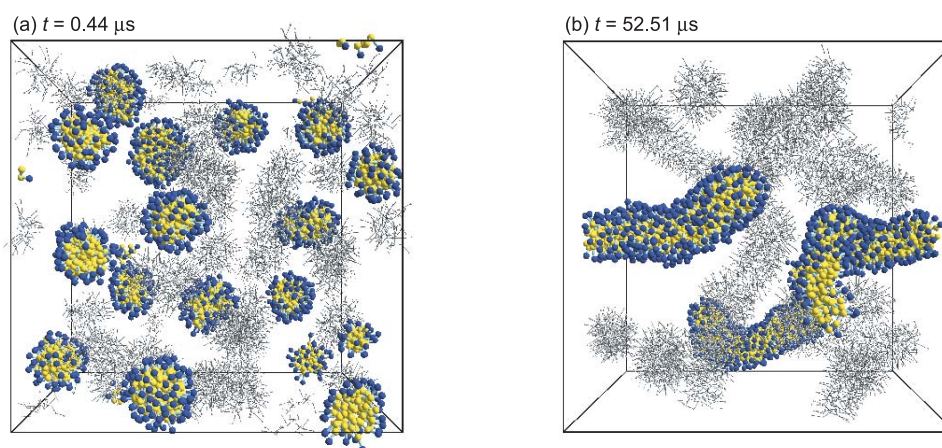


Fig. 1: Snapshot of two stages. (a) the first stage (b) the second stage (note: Water molecules are not displayed and the molecules contained of some micelles are emphasized only.)

References

- [1] H. Yamamuro, K. Koyanagi, and H. Takahashi, *Bull. Chem. Jpn.* **78**, 1884 (2005).
- [2] Y. Zhang, J. Schmidt, Y. Talmon, and J. L. Zakin, *J. Colloid and Interface Sci.* **286**, 696 (2005).
- [3] T. Shikata, H. Hirata, and T. Kotaka, *Langmuir* **4**, 354 (1988).
- [4] T. Shikata and H. Hirata, *Langmuir* **5**, 398 (1989).
- [5] S. Imai and T. Shikata, *J. Colloid Interface Sci.* **244**, 399 (2001).
- [6] S. Yamamoto and S. Hyodo, *J. Chem. Phys.* **122**, 204907 (2005).
- [7] P. J. Hoogerbrugge and J. M. V. A. Koelman, *Europhys. Lett.* **19**, 155 (1992).
- [8] P. Español and P. Warren, *Europhys. Lett.* **30**, 191 (1995).

Particle based modelling of ultrasonic plastification with a yield-stress fluid (simulation and experiments)

Authors: Christian Bretthauer^{1,2}, David Kauzlari¹, Claas Müller², Jan G. Korvink¹

**IMTEK, Albert Ludwig University, D-79110 Freiburg im Breisgau
Department of Microsystems Engineering**

**¹Laboratory for Simulation, ²Laboratory for Process Technology
{bretthau, kauzlari, jan.korvink, claas.mueller}@imtek.uni-freiburg.de**

ABSTRACT

Using ultrasonics for the plastification of thermoplastics has become a standard technique in the field of plastic welding. By the use of ultrasound it is possible to obtain reliable weld seams without heating the connecting parts to their glass transition temperature. We analyse the potential of ultrasound for low temperature plastification of PMMA both theoretically and experimentally. We investigate the ability of yield-stress fluid models to describe the plastification during application of ultrasound correctly. The deformation of the material is simulated by a particle based method, and the plastification behavior is modeled by a modified Bingham fluid. We discuss the general capability of particle simulation as a tool for simulating highly viscous flows on small length scales and propose solutions to overcome the major drawbacks, such as unacceptably small time steps and underestimated speed of sound. For the former we make use of scaling laws to achieve equivalent flow profiles and for the latter we adjust the ultrasonic boundary condition in order to obtain correct shear rates. Furthermore we present a strategy for a natural implementation of ultrasonic boundary conditions in fluid particle methods. Theoretical predictions are compared with new experimental data.

1. Introduction

Although widely-used in the field of plastic welding, the exact mechanism of ultrasonic plastification of thermoplastics is still not entirely understood. It has been reported that ultrasound is able to plasticize thermoplastics even below the glass transition temperature [1] which indicates that an increase in temperature due to frictional heating is not the only reason for plastification. From polymer melts it is well known that the shear rate has a strong influence on the viscosity. We thus propose that the ultrasound leads to such high shear rates and that the polymer softens even below the glass transition temperature. Simulations of the softening process may help to justify this assumption. We apply particle based fluid simulation methods which have become quite popular these days. One advantage is their ability to model free surface flows and large deformations, which is why they seem to be an ideal simulation tool for simulating the deformation during the ultrasonic plastification process. Dissipative Particle Dynamics (DPD) is one possible choice. It includes mesoscopic fluctuations in its momentum and energy equations. These fluctuations do not play a major role for the simulation of highly viscous fluids but the algorithm has shown to be stable and is thus a straight-forward approach for the simulation of the plastification process.

2. Simulation parameters and boundary conditions

The standard DPD approach is as follows: a fluid or gas is represented by particles, each characterized by a position \mathbf{r}_i , velocity \mathbf{v}_i and in case of energy conservation also an internal energy ε_i . There are three different kinds of forces acting between the particles, namely the conservative force \mathbf{F}_{ij}^C , the dissipative force \mathbf{F}_{ij}^D and the random force \mathbf{F}_{ij}^R , where the indices identify the particles' reference numbers. To reduce the computational effort, the range of the forces is limited to a cut-off length r_c . The principles of mass m , momentum \mathbf{p} and energy conservation lead to the update equations

$$\dot{\mathbf{r}}_i = \frac{\mathbf{p}_i}{m_i}, \quad \dot{\mathbf{p}}_i = \sum_{j \neq i} (\mathbf{F}_{ij}^C + \mathbf{F}_{ij}^D + \mathbf{F}_{ij}^R), \quad \dot{\varepsilon}_i = \sum_{j \neq i} q_{ij}, \quad (1)$$

where q_{ij} denotes a generalized heat flux, including frictional heating as well as heat conduction [2]. The fluid's equation of state (EOS) is defined by the conservative forces. We decide to follow Warren [3] and use a force given by

$$\mathbf{F}_{ij}^C = (A\omega^A + B(\rho_i + \rho_j)\omega^B)\mathbf{e}_{ij} \quad (2)$$

with local densities ρ_i, ρ_j , and the unit vector $\mathbf{e}_{ij} = \mathbf{r}_{ij}/r_{ij}$ pointing from particle j to particle i . The weighting functions ω^A and ω^B depend on the absolute distance r_{ij} and incorporate cut-off radii of $r_c^A = 1$ and $r_c^B = 0.75$. For force amplitudes of $A < 0$ and $B > 0$, the resulting EOS was found to be

$$p = \rho k_B T + \alpha A \rho^2 + 2\alpha B r_c^{B^4} (\rho^3 - c\rho^2 + d) \quad (3)$$

with pressure p , virial coefficient $\alpha = 0.101$, fit parameters c and d , temperature T and Boltzmann constant k_B [4]. Starting from this equation we determine appropriate values for A and B in order to fit the correct compressibility κ of PMMA. As a rule of thumb the cut-off length should be at least 3 times larger than the typical inter particle distance $\lambda \approx \rho^{-1/3}$ [4]. For a cut-off radius of unity this leads to a minimum equilibrium density of $\rho = 27$ in DPD units. Unfortunately it is practically impossible to fit the real compressibility and sonic velocity due to the soft conservative forces. We therefore settle to match a dimensionless compressibility

$$\kappa_{DL}^{-1} = \frac{1}{nk_B T \kappa_{PMMA}} = \frac{1}{k_B T} \left(\frac{\partial p}{\partial \rho} \right)_T = \frac{k_B T + 2\alpha A \rho + 2\alpha r_c^{B^4} B(3\rho^2 - 2c\rho)}{k_B T} \quad (4)$$

where n denotes the molecular number density of the polymer. We observe that, although the sonic velocity due to the conservative forces only is about three orders of magnitude too small, it is enhanced in turn by the high bulk viscosity arising from the dissipative forces described below such that the total sonic velocity is only one order of magnitude too small.

Dissipative forces affect the viscosity of a DPD fluid, by leveling velocity differences of adjacent particles, and therefore lead to a balancing of the momentum distribution. Instead of using a dissipative force we use an energy conserving Peters-thermostat [5]. It relaxes the relative velocities of pairs of particles to a fraction $\alpha_{ij} = 1 - \exp[-2\gamma_{ij}\omega(r_{ij})\Delta t]$, where γ_{ij} is an adjustable dissipation constant of the thermostat, ω is again a weighting function and Δt is the time step length. The thermostat redistributes the change in the kinetic energy equally to the

internal energy of both particles. Eqn. 5. shows the dependence of the viscosity on the time step and the dissipation constant γ of the thermostat, where c_1 , c_2 and c_3 denote fit constants.

$$\eta \approx \frac{c_1}{\Delta t} \left(1 - \exp[-c_2 \gamma \Delta t] + \sqrt{1 - \exp[-2c_2 \gamma \Delta t]} \right) + c_3 \quad (5)$$

Note that by increasing the relaxation frequency $1/\Delta t$ we are able not only to increase the maximum viscosity, but also to obtain a wider viscosity bandwidth. Since we are aiming at simulating a softening process we choose a time step of $\Delta t = 10^{-5}$ in DPD units which provides us with a viscosity-bandwidth of about two orders of magnitude. To simulate on micrometer length scales and viscosities of the order of 10^5 Pa s as it is necessary for polymer flows we would need to resolve time steps of 10^{-13} s. This is obviously not pragmatic and we therefore propose to perform an equivalent flow simulation instead. The underlying idea is to set the ratio of clamping pressure and viscosity to the correct value by reducing the pressure. To describe the softening behavior of PMMA under the influence of ultrasound we introduce a modified Bingham model incorporating both yield-stress and shear thinning. The viscosity is a function of the temperature and the shear rate $\dot{\gamma}$, given by

$$\eta(T, \dot{\gamma}) = \eta_1 \cdot \exp[-t_1 \dot{\gamma}] + \frac{\tau_0}{2} \left(1 / \left(1 + \exp\left[\frac{\dot{\gamma} - \dot{\gamma}_c}{t_2}\right] \right) + 1 / \left(1 + \exp\left[\frac{T - T_c}{E_a / k_B T}\right] \right) \right). \quad (6)$$

Exceeding the critical values $\dot{\gamma}_c$ and T_c for the shear rate and temperature respectively causes the viscosity to drop. The parameters t_2 and E_a define the slope of this viscosity drop in dependence of $\dot{\gamma}$ and T , respectively, while η_1 and τ_0 define the maximum viscosity. Shear thinning behavior is captured by the first term with the constant t_1 . In order to include this viscosity model in MDPD we replaced η in Eqn.5 by Eqn.6 and solved for the dissipation constant. This leads to a dissipation constant for the Peters-thermostat as a function of the respective particle's temperature and shear rate.

Walls in DPD simulations can be modeled by “frozen” particles which are placed behind the wall. We realized ultrasonic boundary conditions by introducing an oscillating velocity for the wall particles representing the vibration of the walls. Since the particles do not move, the ultrasonic coupling is of purely frictional character.

3. Ultrasonic plastification simulations and experiments

To investigate the softening process we use an ultrasonic welding machine *ES 35* from Ultrasonics[®] with an ultrasonic frequency of 35 kHz and a maximum power of 1kW. An ultrasonic horn was designed with micro pillars at the tip to investigate the filling of the gaps due to the plastification process. For the simulations we use only a cut-out of this geometry (see Fig.1) to save simulation time. The wall particles are kept at a constant temperature of 25°C to account for the large heat conduction of the brass horn. The oscillation direction is along the axis of the pillars (indicated by the thick double arrow).

Fig. 1 shows the simulation and experimental results after one second of ultrasound with an intensity of 180 dB. As can be seen, the highest temperature is about 100°C. This shows the capability of ultrasound to plastify PMMA below the glass transition temperature of 120°C. Experimental observations support these simulation results.

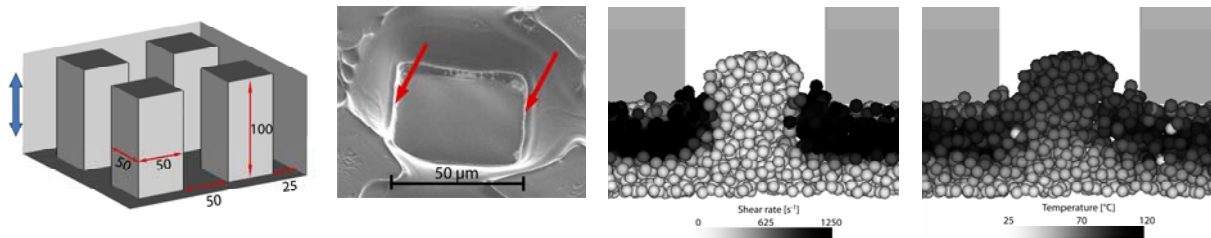


Figure 1. From left to right: Test geometry; partially filled structure; simulation results for the shear rate and temperature distribution after application of ultrasound with an intensity of 180dB for one second.

Additionally, we can see a step in the flow profile (see arrows in Fig. 1) in both the simulations and the experiments. Apparently the high heat conduction of the wall prevents a boundary layer of the fluid from heating up to the critical temperature and thus inhibits faster flow.

4. Summary

We investigated ultrasonic plastification of PMMA, both experimentally and theoretically. By including a modified Bingham fluid into MDPD simulations it was possible to obtain qualitative agreement with experimental data. Our simulations indicate yielding due to high shear rates to be responsible for the decrease in the necessary process temperature for ultrasonic plastification compared to conventional plastification.

References

- [1] T. Kunihiro and T. Hirokazu, 1998, “Molecular movement during welding for engineering plastics using Langevin transducer equipped with half-wave-length step horn”, *Ultrasonics*, **36**, 75-78.
- [2] P. Espanol, M. Ripoll and Matthieu H. Ernst, 1999, “Dissipative particle dynamics with energy conservation: Heat conduction”, *Int. J. Mod. Phys. C*, **9**(8), 1329-1338.
- [3] P. B. Warren, 2003, “Vapor-liquid coexistence in many-body dissipative particle dynamics”, *Phys. Rev. E*, **68**, 066702.
- [4] R. Groot and P. B. Warren, 1997, “Dissipative particle dynamics: bridging the gap between atomistic and mesoscopic simulation”, *J. Chem. Phys.*, 0021-9606(97)51335-3.
- [5] P. Espanol and M. Ravenga, 2003, “Smoothed dissipative particle dynamics”, *Phys. Rev. E*, **67**, 026705.
- [6] L. Pastewka, D. Kauzlarić, Andreas Greiner and Jan G. Korvink, 2006, “Thermostat with a local heat-bath coupling for exact energy conservation in dissipative particle dynamics”, *Phys. Rev. E*, **73**, 037701.

Computer Simulations of the Dynamics of Polymer Solutions

Burkhard Dünweg

Max Planck Institute for Polymer Research, Ackermannweg 10,
D-55128 Mainz, Germany; duenweg@mpip-mainz.mpg.de

ABSTRACT

A method for simulating the dynamics of polymer–solvent systems is described. The fluid is simulated via lattice Boltzmann and the polymer chains via Molecular Dynamics. The two parts are coupled by a simple dissipative point–particle force, and the system is driven by Langevin stochastic forces added to both the fluid and the polymers. This method is applied to a semidilute system of chains of length $N = 1000$. We observe the crossover from Zimm dynamics at short length and time scales to Rouse dynamics at long length and time scales. Moreover, we find “incomplete screening”, i. e. Zimm–like behavior at short times but large length scales. This behavior can be nicely described in terms of the de Gennes picture, which explains hydrodynamic screening as a result of entanglements. An analogous simulation approach has been developed for electrostatics, where the interaction is described by a dynamic Maxwell field coupled to the system of charges. This method will be briefly outlined as well, with emphasis on the analogy between hydrodynamics and electrostatics.

1. Hydrodynamic Interactions: A Computational Challenge

Complex fluids like colloidal dispersions or polymer solutions are characterized by a huge difference in length scales and, even more importantly, time scales. The solvent particles are much smaller, and they relax much more quickly, than the solute. Indeed, for a single flexible polymer chain in dilute solution, the macromolecule’s relaxation time may be estimated by the scaling prediction of the Zimm model [1],

$$\tau_Z \sim \frac{\eta R^3}{k_B T}, \quad (1)$$

where η denotes the solvent viscosity, R the chain’s size (e. g. given by the gyration radius), k_B the Boltzmann constant, and T the absolute temperature. The underlying picture is a self–similar object relaxing on all length scales λ , where the corresponding relaxation time is given by $\tau(\lambda) \sim \eta \lambda^3 / (k_B T)$, implying a dynamic exponent $z = 3$. The longest relaxation time is given by the time which the object needs to move its own size, and this is in turn governed by its diffusion constant D : $D \tau_Z \sim R^2$. Equation 1 then follows from the fact that the chain behaves essentially like a Stokes sphere, as far as diffusion is concerned, $D \sim k_B T / (\eta R)$.

The important point for computer simulations is that Eq. 1 holds (approximately) for the solvent particles as well; however, the relaxation is much faster. Thus, a length scale ratio of, say, only ten would result in a chain relaxation which is

roughly one thousand times slower than that of the solvent particles, or of the monomers. Therefore simulations of polymer dynamics which aim at resolving the full spectrum of relaxation times between the monomer scale and the macromolecular scale are intrinsically expensive, and one would like to do this with a model / method which is as simple and efficient as possible.

The most striking observation is that for dilute systems there are many more solvent than solute degrees of freedom. Therefore the solvent should be reduced to its bare essentials, which are just needed to reproduce the chain dynamics correctly. The first important solvent property is the supply of thermal noise, such that one is tempted to just simulate the solute particles via Brownian Dynamics,

$$\dot{\vec{r}}_i = \frac{1}{\zeta} \vec{F}_i + \vec{f}_i, \quad (2)$$

where ζ is the friction coefficient of monomer i at position \vec{r}_i , \vec{F}_i the deterministic force, and \vec{f}_i the Langevin noise. However, this simple scheme does not take into account the *hydrodynamic interaction*, which is nothing but *highly correlated* motion of the Brownian particles, due to fast diffusive momentum transport through the solvent, and of paramount importance for dilute systems. These correlations are actually the reason for the Stokes-like behavior of the diffusion constant; without them one would obtain Rouse-like scaling $D \propto N^{-1}$, where N is the degree of polymerization. The so-called Schmidt number $Sc = \eta_{kin}/D_m$, i. e. the ratio between kinematic viscosity (which is the diffusion constant for momentum) and monomer diffusion coefficient, has typical values of $10^2 \dots 10^3$ in dense fluids, and can safely be replaced by $Sc = \infty$. Therefore, one should replace Eq. 2 by

$$\dot{\vec{r}}_i = \sum_{ij} \overleftrightarrow{\mu}_{ij} \vec{F}_j + \vec{f}_i, \quad (3)$$

where the Langevin noise is now described by a huge correlation matrix, proportional to the mobility matrix $\overleftrightarrow{\mu}_{ij}$,

$$\langle \vec{f}_i(t) \otimes \vec{f}_j(t') \rangle = 2k_B T \overleftrightarrow{\mu}_{ij} \delta(t - t'). \quad (4)$$

$\overleftrightarrow{\mu}_{ij}$ can be calculated from hydrodynamics [1] with various degrees of accuracy (Oseen-Tensor, Rotne-Prager-Tensor, etc.); the leading-order Oseen correlations are long-ranged, decaying like $1/r$. The Oseen tensor is nothing but the Green's function of the Stokes equation, in close analogy to electrostatics, where the Coulomb potential is the Green's function of the Poisson equation. This matrix has been a severe obstacle to Brownian dynamics simulations, since simple algorithms to treat it scale as N^3 , where N is the number of Brownian particles. Recent progress has reduced this to roughly $N \log N$ [2]; however, this complicated method has not yet found widespread use.

The "mesoscopic" approach instead resolves this problem by *keeping* the solvent degrees of freedom, but reducing them to just a means of momentum transport. Different methods (Navier-Stokes, Dissipative Particle Dynamics [3], Multi-Particle Collision Dynamics [4], lattice Boltzmann (LB) [5]) have been invented and implemented, and in the author's opinion they are all very similar both in terms

of philosophy and (probably) computational efficiency. Space restrictions do not permit to describe any of these here. For complex fluids, one then couples one such method to a particle description of the solute, making sure that the overall momentum is conserved. An important point is that the solvent should be *structureless*, in order to make sure that the static equilibrium properties of the solute are the same with and without solvent, such that the latter can be discarded for equilibration.

The method developed in our group [6] is based upon a simple LB description for the solvent, coupled dissipatively to a bead–spring system to describe polymers. The latter is described by the equation of motion

$$m\ddot{\vec{r}}_i = \vec{F}_i - \zeta \left(\dot{\vec{r}}_i - \vec{u}(\vec{r}_i) \right) + \vec{f}_i, \quad (5)$$

where \vec{f}_i is a standard Langevin noise, while $\vec{u}(\vec{r}_i)$ is the solvent velocity at the particle’s position, obtained via linear interpolation from the surrounding lattice sites. The LB part is subjected to a fluctuating Langevin stress tensor, and external forces coming from the Brownian particles (these forces are determined via interpolating back onto the lattice, plus the condition that the overall momentum should be conserved). This system satisfies the fluctuation–dissipation theorem, and faithfully represents hydrodynamic interactions on sufficiently large length and time scales. The Schmidt number can be chosen as rather large (roughly 0.5×10^2), by using a suitably large value for ζ .

2. Hydrodynamic Screening in Semidilute Polymer Solutions

A semidilute polymer solution (in good solvent) is characterized by the so-called “blob size” ξ [7], which marks the onset of chain–chain interactions, and which governs *both* the static crossover from self–avoiding walk (SAW) statistics at small length scales to random walk (RW) statistics at large length scales, *and* the dynamic crossover from Zimm dynamics for small length scales to Rouse dynamics at large length scales. This latter crossover, which is usually referred to by the term “hydrodynamic screening”, had been poorly understood. An important landmark was the observation by de Gennes [8] that the screening is due to *entanglements*, which, in the present context, should however not be viewed as topological confining interactions as in reptation theory [1], but rather as the presence of chain–chain collisions. In this picture, the blobs are viewed as “hooked up” in a temporary gel, such that they provide Darcy–type friction to the solvent flow. Thus the viscous stress $\eta \nabla^2 \vec{u}$ in the Stokes equation should be augmented by an additional term $-\zeta_{blob} c_{blob} \vec{u}$, where ζ_{blob} is the friction constant of a blob, and c_{blob} the concentration of blobs. However, since $c_{blob} \sim \xi^{-3}$, and $\zeta_{blob} \sim \eta \xi$ (Stokes), this term can also be written as $(\eta/\xi^2) \vec{u}$. Balancing this against the viscous stress, one finds a hydrodynamic screening length $\sim \xi$. Therefore, there are no hydrodynamic correlations beyond the length scale ξ , such that the dynamics should be Rouse–like there.

Our simulation data [9] show that this picture needs to be completed in terms of time scales. Though the Darcy picture of screening by the blobs turns out

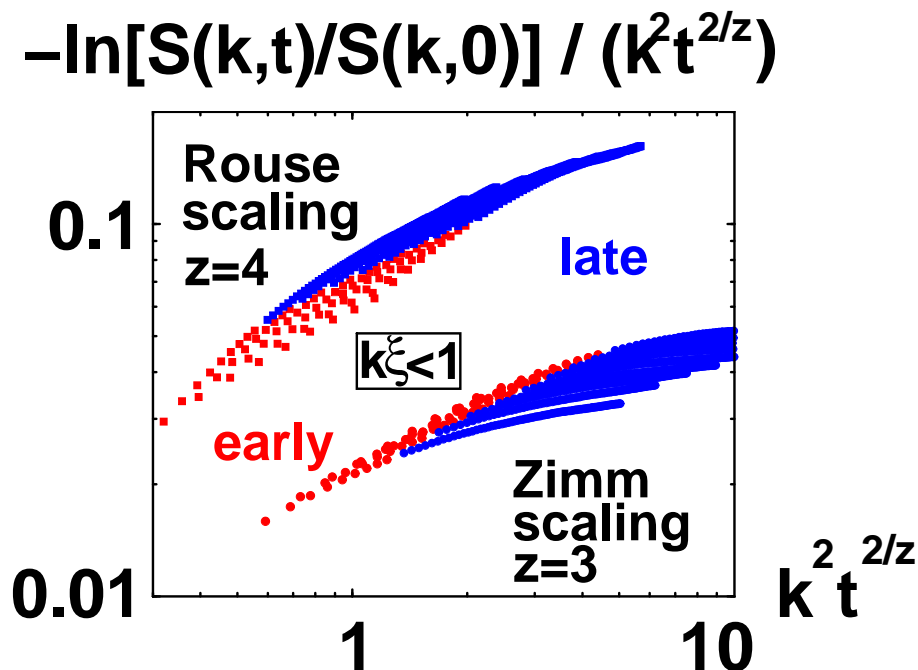


Figure 1: Single-chain dynamic structure factor $S(k, t)$ for a semidilute polymer solution (replotted data of Ref. [9]). The wave numbers k are restricted to the regime $k\xi < 1$, such that only correlations beyond the blob size are probed. For pure Zimm scaling, the structure factor should be just a function of $k^2 t^{2/3}$, while it should only depend on $k^2 t^{1/2}$ for pure Rouse scaling. The early and late times refer to those which are smaller or larger than τ_ξ .

to be essentially correct, one nevertheless needs to take into account that the entanglements are not felt before the blob relaxation time $\tau_\xi \sim \eta\xi^3/(k_B T)$, which is the average waiting time until a chain-chain collision occurs. Before this time, an initial “kick” will just propagate throughout the system, and just drag the chains along. Therefore, the hydrodynamic interactions are *unscreened* on time scales below τ_ξ , even on large length scales well beyond ξ . This completes the de Gennes picture, and explains the experimental observation of “incomplete screening” [10] in a straightforward way.

It should also be mentioned that this study was quite non-trivial with respect to computational demands: In order to resolve the SAW-RW crossover, and the Zimm-Rouse crossover, we needed roughly thirty blobs per chain, plus roughly thirty monomers per blob, such that we needed to simulate 50 chains of length 1000 in a box containing 88^3 LB lattice sites. This is the smallest system one can study for this problem.

3. Maxwell Equations Molecular Dynamics (MEMD)

For hydrodynamic interactions, we started from the observation that the $1/r$ Oseen tensor is just the Green’s function of a dynamic field theory (hydrodynamics) in its

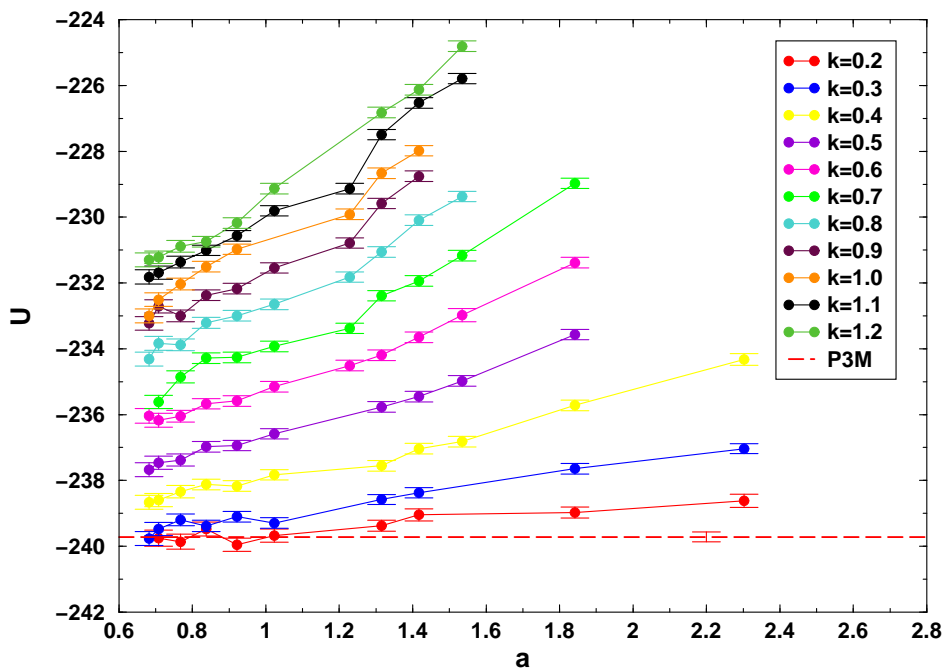


Figure 2: Electrostatic energy of a system of 4000 particles interacting via purely repulsive Lennard–Jones (LJ) interactions, and electrostatics. The Bjerrum length $l_B = e^2/(4\pi\epsilon_0 k_B T)$ has the value 2.5 in units of the LJ parameter, which also defines the unit of length for the lattice spacing a (parameter of the abscissa), and the screening parameter κ of the artificial Yukawa field theory. The density has the rather small value 10^{-2} . In the continuum limit $a \rightarrow 0$, the results all converge to the exact value, which was obtained by accurate P³M simulations.

quasistatic limit, and that we can construct an efficient algorithm by going back to the original dynamic field theory, i. e. by coupling the Brownian particles to the Navier–Stokes velocity field, such that the interaction comes about by propagation of the latter. Nothing prevents us from applying the same philosophy to the Coulomb interaction between charged particles, which we couple straightforwardly to a propagating Maxwell field. This idea has been put forward by A. Maggs, and also pursued by us [11] (see also references in there). Since the approach has been described in detail in Ref. [11], we wish to be brief, and just outline the main features:

(i) Again the charges move in continuum space, while the electric and magnetic fields live on a simple–cubic lattice. (ii) The charges are linearly interpolated onto the nodes of the lattice, while current density \vec{j} , electric field \vec{E} , and magnetic vector potential \vec{A} are objects associated with the connecting links. (iii) This scheme allows a natural and straightforward discretization of the Maxwell equations. (iv) The discrete analogs of the continuity equation, and Gauss’ law, are satisfied within machine accuracy. (v) The equations of electrostatics $\nabla \cdot \vec{E} = \rho/\epsilon_0$, $\nabla \times \vec{E} = 0$ can be mapped onto a variational problem, where the electrostatic field energy $(\epsilon_0/2) \int d^3\vec{r} \vec{E}^2$ is minimized under the constraint of Gauss’ law. This is analogous

to quantum–mechanical density functional theory, where the density functional needs to be minimized. (vi) Replacing the minimization by some Hamiltonian dynamics is exactly the approach of Car and Parrinello; MEMD can be shown to be formally very close related, with $1/c^2$ (c speed of light) an adjustable mass–like parameter, whose value is irrelevant for the static averages in thermal equilibrium, while $c/v \approx 20$ (v particle velocity) seems to be sufficient to also obtain reasonable dynamics. (vii) The distribution of particles onto lattice sites introduces an unphysical self–interaction, which however can be approximately (within time step errors) subtracted, using the appropriate lattice Green’s function. (viii) A combination with an artificial Yukawa–type field theory allows us to use the same trick as for Ewald sums, i. e. the interactions are evaluated directly in real space for short distances, while the Maxwell field propagation ensures proper Coulomb interactions on the larger length scales. (ix) With this trick, it is possible to treat dilute systems with a rather coarse grid, such that the method does not suffer from inefficiency even in this limit. (x) Preliminary benchmarks seem to indicate that the method is quite competitive with conventional electrostatics solvers like P³M, while having very advantageous properties with respect to scaling, parallelizability, and ease of implementation.

Acknowledgements

It is my pleasure to thank Patrick Ahlrichs and Igor Pasichnyk, on whose work the present article is built.

References

- [1] M. Doi and S. F. Edwards. *The Theory of Polymer Dynamics*. Oxford University Press, Oxford (1986).
- [2] A. J. Banchio and J. F. Brady. *Accelerated Stokesian dynamics: Brownian motion*. J. Chem. Phys. **118**, 10323 (2003).
- [3] P. Español and P. Warren. *Statistical mechanics of dissipative particle dynamics*. Europhys. Lett. **30**, 191 (1995).
- [4] A. Malevanets and R. Kapral. *Mesoscopic model for solvent dynamics*. J. Chem. Phys. **110**, 8605 (1999).
- [5] S. Succi. *The Lattice Boltzmann Equation for Fluid Dynamics and Beyond*. Oxford University Press, Oxford (2001).
- [6] P. Ahlrichs and B. Dünweg. *Simulation of a single polymer chain in solution by combining lattice Boltzmann and molecular dynamics*. J. Chem. Phys. **111**, 8225 (1999).
- [7] P. G. de Gennes. *Scaling Concepts in Polymer Physics*. Cornell University Press, Ithaca (1979).

- [8] P.-G. de Gennes. *Dynamics of entangled polymer solutions. 2. Inclusion of hydrodynamic interactions.* *Macromolecules* **9**, 594 (1976).
- [9] P. Ahlrichs, R. Everaers, and B. Dünweg. *Screening of hydrodynamic interactions in semidilute polymer solutions: A computer simulation study.* *Phys. Rev. E* **64**, 040501 (R) (2001).
- [10] D. Richter, K. Binder, B. Ewen, and B. Stühn. *Screening of hydrodynamic interactions in dense polymer solutions: A phenomenological theory and neutron scattering investigations.* *J. Phys. Chem.* **88**, 6618 (1984).
- [11] I. Pasichnyk and B. Dünweg. *Coulomb interactions via local dynamics: A Molecular-Dynamics algorithm.* *J. Phys.: Cond. Matt.* **16**, S3999 (2004).

Atomistic, Mesoscale And Finite Element Techniques For Polymer Materials Simulations

Gerhard Goldbeck-Wood¹, James Wescott¹, Reinier Akkermans¹, Amitesh Maiti²

¹ Accelrys Ltd, 334 Cambridge Science Park, Cambridge, CB4 0WN, UK, gerhard@accelrys.com; ² Chemistry and Materials Science Directorate, Lawrence Livermore National Laboratory, P.O. Box 808, L-090, Livermore, CA 94551, maiti2@llnl.gov.

ABSTRACT

We present advances in Materials Studio ® [1] based methods and applications aimed at determining nanoscale structure and properties of polymer-based materials and composites. On the atomistic scale, an extension of the Monte Carlo based technique called Blends [1] for determining interaction parameters has been evaluated, which accounts for non-configurational entropy contributions. On the mesoscale, we present applications to self-assembling and composite systems using mesoscale and finite element methods. Using MesoDyn [1] we have simulated discrete temperature-dependent transitions of amphiphilic dendron molecules similar to those previously reported in experiments by Wiesner et al [2], and using Dissipative Particle Dynamics (DPD) [1] examined the dispersion of nanotubes in polymer composites. The thermal and electrical conductivity of these systems have been estimated using the MesoProp [1] finite element approach. Finally, a new mesostructure builder tool in Materials Studio is introduced, and applied to a study of phase-separation within diblock copolymer nanodroplets, comparing new DPD results with published MesoDyn simulations [3].

1. Determination of interaction parameters

The effective interaction between different species as required by mesoscale methods such as DPD and MesoDyn, is often parametrized by the Flory-Huggins χ -parameter. The χ – parameter may be estimated from the pure component solubilities using a mixing rule. Mixing rules, however, are empirical and not always available. A less empirical description is provided by the module Blends [1], a forcefield method that samples the energy of molecular pairs. Since every combination of species is considered, no mixing rule is required. Packing effects are accounted for through coordination numbers. Since only the energy of molecular pairs is required, Blends is a very efficient way to calculate χ -parameters. Although qualitatively useful, quantitative prediction is relatively poor. A possible improvement of the method is to include entropic contributions of the pair interactions into the parameter. This can be done in a straightforward manner, as follows.

The χ -parameter, which in Blends is given by

$$\chi_{ij} = \frac{1}{2} \beta \left((z_{ij} + z_{ji}) \epsilon_{ij} - z_{ii} \epsilon_{ii} - z_{jj} \epsilon_{jj} \right) \quad (1)$$

is instead determined by

$$\chi_{ij} = \frac{1}{2} \beta \left((z_{ij} + z_{ji}) a_{ij} - z_{ii} a_{ii} - z_{jj} a_{jj} \right) \quad (2)$$

where a_{ij} is the free energy of a pair of molecules, given by the partition function, which itself results from the density of states $g(\epsilon)$ readily available from the simulation.

$$\beta a_{ij} = - \ln \int d \epsilon g_{ij} \exp(- \beta \epsilon) \quad (3)$$

First results from calculations on a range of polymers are encouraging, as shown in Fig 1.

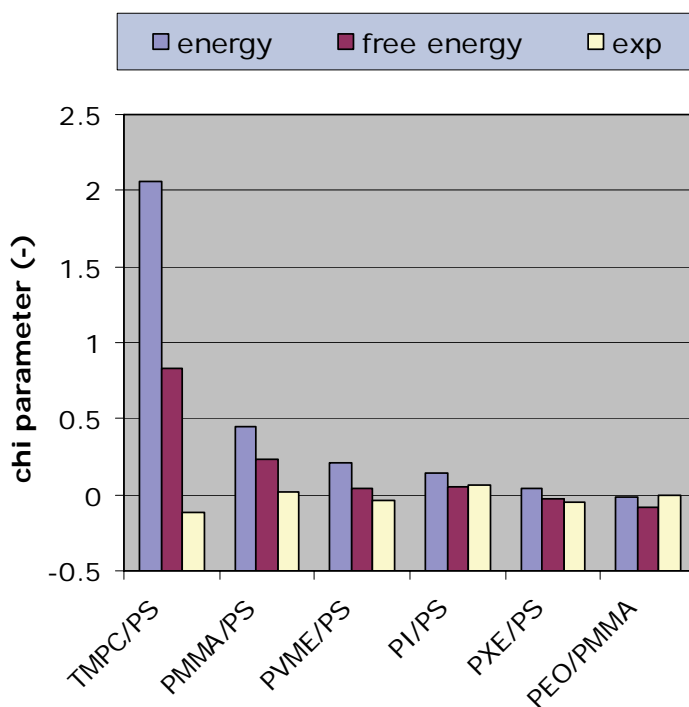


Figure 1: χ -parameters of a range of polymer blends, comparison of experiment [4] with simulations based on the energy, Eqn (1), and the new free energy approach, Eqn (2).

2. Phase transitions in Dendron systems

Wiesner et al [2] studied the self-assembly of amphiphilic dendrons extended with linear polyethylene oxide (PEO) chains and their ion complexes. It is thought that keeping the dendron core and linear PEO chain compatible allows for the combination of dendritic core-shell and conventional block copolymer characteristics for complex mesophase behaviour. An unexpected sequence of crystalline lamellar, cubic micellar, hexagonal columnar, continuous cubic, and lamellar mesophases as is observed with increasing temperature. This is thought to be because dendrons introduce curvature to the interfaces of regular diblock copolymer phases. Greater understanding of the factors controlling the formation of these phases is the aim of our simulations.

The very simple dendron model shown in Fig. 2 reproduces the micellar and lamellar phases of the experimental work but does not appear to properly produce the hexagonal or continuous cubic phases. We have therefore investigated alternative models including one using two beads to represent the branches and hydrophilic beads that extend further into the core of the dendron. As a result, a stable and structured bicontinuous phase is found, suggesting that the penetration of PEO units into the core of the dendron is a key structural element for obtaining the complex phase behaviour of these dendron systems.

A comparison of the temperature at which we find the onset of a disordered phase in different types of dendrons also suggests the model is capturing the essential physics of this system.

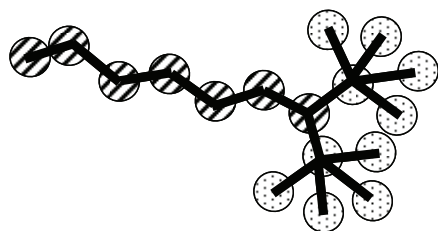


Figure 2: A coarse-grained of a dendron molecule as input to MesoDyn. Each bead represents several monomers, and there are two bead types: PEO type (striped), and PE type (dotted).

In addition to the structural studies, the finite element method MesoProp [1] has been used to characterise the effect of the morphology on properties such as conductivity.

3. Dispersion of nanotubes in polymer composites

Controlling the dispersion of carbon nanotubes (CNTs) in solvent or in polymers is often the largest technological barrier in the development of advanced CNT-based materials. Modelling and simulation could guide experimental efforts by showing if it is possible to process CNTs in a specific environment, or whether significant enhancement of physical properties is possible with the addition of very small quantities of CNTs.

We have previously [5,6] approached the problem of dispersion of CNTs in homopolymers from the perspective of Flory-Huggins theory. Here we investigate how immersion into thin films of block co-polymer melts may be used to control the dispersion of CNTs. Composites have been found to self-assemble into interesting patterns, including percolating networks at low fractions of CNT content. The MesoProp [1] approach was used to estimate the enhancement of important physical properties as a function of CNT concentration.

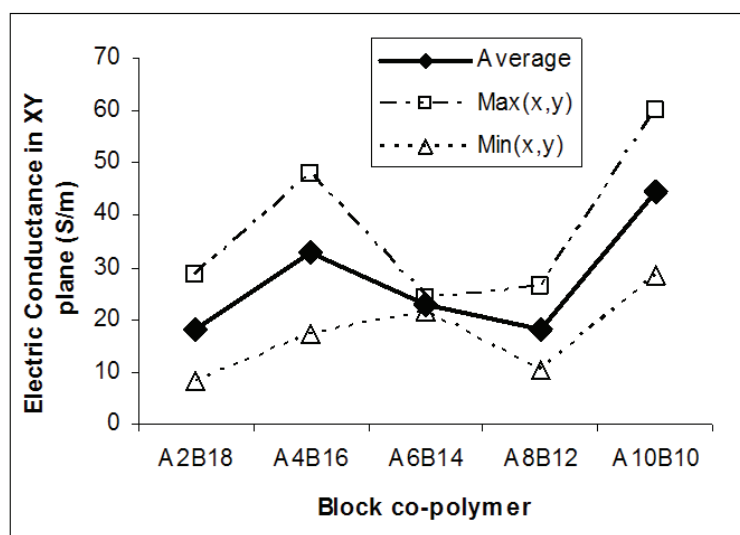


Figure 3. Average electric conductance in the plane of thin films for block copolymer – nanotube composites at 1 vol% fraction of CNTs. x and y in the Max(x,y) and Min(x,y) labels correspond to the two directions in the plane.

We find that the electric conductance depends on percolation of nanotubes across the polymer layer. This is a dynamic process as connections form and break. The threshold for any conductance to occur is about ½ vol% CNT. There is a non-trivial dependence of percolation

on the underlying block copolymer morphology. CNTs are preferentially wetted by the A polymer, but bridges across the B polymer form to complete the network (Fig. 3). Several length scales are important, the ratio of CNT length to the distance between A- regions being the most important. In some cases, such as for A6B14, the distribution of A-polymer frustrates the formation of a percolated network of CNTs at concentrations below 5 vol%.

4. Phase separation inside block copolymer nanodroplets

The morphology of nano-structured soft materials depends not only on the self-assembly behaviour of the components such as amphiphilic block-copolymers, but also on the assembly pathways as determined by external fields, as well as the initial starting structures. A case in point is that of polymer surfactant droplets dispersed in a weak solvent environment. Phase separation inside these droplets has been found in self-consistent field simulation based on the MesoDyn method, including a perforated structure resembling buckyballs [3].

In Materials Studio, a new tool has been implemented to build complex initial mesoscale structures. Simulations of nanodroplets under the same conditions as in Ref [3], but using the DPD code, show a similar range of structures, but with somewhat more defects. As an example, the perforated structure found for the A14B6 block copolymer is shown in Fig. 4.

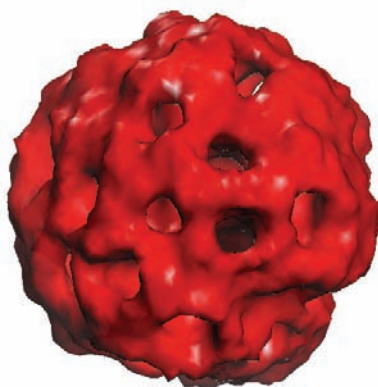


Figure 4. Morphology of a A14B6 polymer surfactant, showing the isosurface of the solvophobic A component.

References

- [1] Materials Studio ® by Accelrys Software Inc, San Diego, CA. See <http://www.accelrys.com/products/mstudio/> and links for all products in Materials Studio including DPD, MesoDyn, Blends and MesoProp
- [2] B.-K. Cho, A. Jain, S. M. Gruner and U. Wiesner Science **305**, 1598 (2004).
- [3] J. G. E. M. Fraaije and G. J. A. Sevink, Macromolecules **36**, 7891 (2003).
- [4] N.P. Balsara, in: Physical Properties of Polymers Handbook, J.E. Mark (ed), Ch. 19, 257, AIP Press, New York (1996).
- [5] A. Maiti, J.T. Wescott and P. Kung, Molecular Simulation **31**, 143 (2005).
- [6] A. Maiti, J. T. Wescott and G. Goldbeck-Wood, Int. J. Nanotechnology, **2**, 198 (2005).

Hierarchical Material Simulation and Coarse Graining

Shi-aki Hyodo

Computational Physics Lab., TOYOTA Central R&D Labs., Inc.
41-1 Aza-Yokomichi, Oaza-Nagakute, Nagakute-cho, Aichi-gun, Aichi-ken, 480-1192,
Japan.
E-mail address: e0668@mosk.tytlabs.co.jp

ABSTRACT

A generalized coarse graining equation of motion was introduced based on the explicit Hamiltonian at the finer hierarchical level and the projection operator technique. Fundamental characteristics were briefly discussed in relation to practical hierarchical material simulations.

1. Introduction

Hierarchical simulation is promising to investigate structures, properties, preferable construction-processes etc. of practical complicated materials. For homogeneous systems, reproduction of local structures/properties has been well studied via averaging the effects of surroundings. Dielectric friction theory of ion transport is a typical example. The reptation theory on the viscoelastic behaviour of concentrate polymer solutions is another one. Our knowledge seems to be already well established to express hierarchical situations. Once we simulate a structure or distribution functions at larger scale, we may reproduce local structures/properties by applying such theories under inhomogeneous surroundings. Several mesoscopic simulations have been proposed and found to be useful. Cooperative simulation at the atomistic and mesoscopic levels would be effective to practical investigations. However, the process on "coarse-graining" has to be investigated more explicitly.

An example of cooperative simulation at the atomistic and mesoscopic levels for a hydrated polyelectrolyte membrane has previously been reported [1, 2]. This hierarchical simulation was performed on the mesoscopic structural formation based on the chemical formula of polyelectrolyte and deduced the electronic state of a hydronium ion in a hydrated membrane. This represents a practical example of an electronic structure calculation under a mesoscopic inhomogeneous environment.

Unfortunately, the above procedure has still stayed at an example of "modeling" on mesoscopic structural simulations. It is therefore required to develop coarse-graining methods which present definite relationship between atomistic and mesoscopic levels. We derived the equation of motion for the coarse-grained (CG) particles by using a projection operator method and calculated the mean force between CG particles by molecular dynamics simulations [3]. This would be a general basis for hierarchical procedure connecting molecular and mesoscopic simulations.

The derived coarse graining equation of motion would be introduced in the present talk. Fundamental characteristics are briefly discussed in relation to practical hierarchical material simulations.

2. Generalized coarse-graining equation of motion

We derived equation of motion for the CG particles by using projection operator method and calculated the mean force between CG particles by molecular dynamics simulations [3]. The idea of coarse-graining we adopt here is to divide the total N_t molecules into N groups (or clusters) which consist of n_α , ($\alpha = 1, \dots, N$) molecules, and regard each molecular group as a CG particle. To derive the equation of motion for the coarse graining particles, we introduce projection operator \mathbf{P} and $\mathbf{Q} = \mathbf{I} - \mathbf{P}$ and divide Liouville equation for $f_s(\hat{\Gamma}_s(t); \Gamma_s)$; the phase space density for CG particles.

$$\frac{\partial}{\partial t} f_s(\hat{\Gamma}_s(t); \Gamma_s) = \mathbf{P}iL f_s(\hat{\Gamma}_s(t); \Gamma_s) + \mathbf{Q}iL f_s(\hat{\Gamma}_s(t); \Gamma_s), \quad (1)$$

where $\hat{\Gamma}_s \equiv \{\hat{\mathbf{R}}_\alpha, \hat{\mathbf{P}}_\alpha\}$ denotes the positions and momenta of the center of mass of the CG particles. We obtained the equation of motion for the CG particles by integration of Eq. (1) with multiplying \mathbf{P}_σ ,

$$\frac{d}{dt} \hat{\mathbf{P}}_\sigma(t) = \sum_{\alpha \neq \sigma} \langle \mathbf{F}_{\alpha\alpha} \rangle_{\Gamma_s} - \frac{\beta}{2} \sum_{\eta \neq \sigma} \sum_{\alpha} \sum_{\beta} \int_0^t ds \langle \delta \mathbf{F}_{\sigma\eta}^{\mathbf{Q}}(t-s)^T \delta \mathbf{F}_{\alpha\beta}^{\mathbf{Q}}(0) \rangle \mathbf{V}_{\alpha\beta} + \sum_{\alpha \neq \sigma} \delta \mathbf{F}_{\sigma\alpha}^{\mathbf{Q}}(t), \quad (2)$$

where $\langle \dots \rangle_{\Gamma_s}$ denotes an average with fixed $\hat{\Gamma}_s$. The meaning of the first, second and third terms are the mean force, the friction force and the microscopic (fluctuating) force, respectively. We also showed correspondence of Eq. (2) to Brownian dynamics and Dissipative Particle Dynamics (DPD). In Eq. (2), all the terms are related to the atomistic information. Then we performed molecular dynamics simulation with such constraint to calculate the mean force. All resulting forces show peaks at some distances and do not diverse even at close distance. Because amount of the mean force should depend on the size of CG particles, it is appropriate to scale the force and distance. The scaled mean forces show universality which correspond to that of the conventional conservative force in DPD.

The projection operator method is a useful technique to eliminate first variables. Although general formulation is given for the coarse-graining via the projection operator, explicit knowledge on the linkage between these formulations and conventional coarse-graining simulation methods has still not been satisfied. Kampen and Oppenheim derived the equation for Brownian motion for single Brownian particle from first principles [4]. Coarse-graining equations for single chain in polymer melt [5], a one-dimensional harmonic chain [6] and three-dimensional harmonic lattices [7] have been also derived using the projection operator method. These derivations are for specific systems, hence farther extension should be advanced. Our resultant equation of motion, Eq. (2), shows explicit linkage between atomistic and mesoscale coarse-graining simulation methods. The information needed to execute the coarse graining simulations can be directory calculated via MD simulations [3].

3. Some fundamental characteristics of the generalized coarse-graining equation of motion

The Liouville operator, L , in Eq. (1) is

$$iL = - \sum_{\alpha} \sum_i \left\{ \frac{\partial H}{\partial \mathbf{r}_{\alpha i}} \frac{\partial}{\partial \mathbf{p}_{\alpha i}} + \frac{\partial H}{\partial \mathbf{p}_{\alpha i}} \frac{\partial}{\partial \mathbf{r}_{\alpha i}} \right\} \quad (3)$$

$$= -\sum_{\alpha} \left\{ \frac{\partial H}{\partial \mathbf{R}_{\alpha}} \frac{\partial}{\partial \mathbf{P}_{\alpha}} + \frac{\partial H}{\partial \mathbf{P}_{\alpha}} \frac{\partial}{\partial \mathbf{R}_{\alpha}} \right\}. \quad (4)$$

Here, H is the Hamiltonian of entire system, $\mathbf{r}_{\alpha i}$ and $\mathbf{p}_{\alpha i}$ are the position and momentum, respectively, of each finer particle i constructing a CG particle α ,

$$\mathbf{R}_{\alpha} \equiv \sum_i m_{\alpha i} \mathbf{r}_{\alpha i} / M_{\alpha}, \quad \mathbf{P}_{\alpha} \equiv \sum_i \mathbf{p}_{\alpha i}, \quad \text{and} \quad M_{\alpha} \equiv \sum_i m_{\alpha i}. \quad (5)$$

The position and momentum of center of mass for a CG particle include all information about internal degrees of freedom here. Equation (1) was derived via the projection operator to extract the information for the center of mass and to treat other degrees of freedom statistically. If there is only one CG particle in the space, all the degrees of freedom can be separated into the motion of center of mass, orientations, and internal vibrations according to the standard theory of molecular vibration-rotation spectroscopy [8]. In this sense, the motion of center of mass is completely separated from orientations and internal vibrations. On the other hand, orientations and internal vibrations commonly correlate as is well-known as the Coriolis interaction and the centrifugal distortion [8]. Applying the projection operator for extracting the motion of center of mass is trivial but for orientation or specific internal vibration is effective in the case of single CG particle. We can therefore understand that the operation on Eq. (1) corresponds to coarse-graining to the effects of orientational motions and internal vibrations of other CG particles. Extension to extracting another degree of freedom, e.g., orientation for dipole correlation etc., could be performed via almost identical procedure to reproduce Eq. (2). We do not need to restrict the third term of Eq. (2) to only random force, because internal vibrations can be defined in each CG particle. When we define the number of degree of freedom is not so large in each CG particle, we can keep an explicit relation between the equations of motion at the CG and finer hierarchical level. This is an appropriate situation for trying practical hierarchical material simulation having the ability for both way transformations of information. When we define the third term of Eq. (2), we can obtain conventional coarse graining equations of motion, e.g., Brownian dynamics or DPD.

Acknowledgements

The author is grateful to Dr. T. Kinjo for his enthusiastic collaboration. He also would acknowledge to Dr. K. Kuramoto for discussing on applications of the coarse-graining equation of motion. A part of this work was supported by NAREGI Nanoscience Project, Ministry of Education, Culture, Sports, Science and Technology, Japan.

References

- [1] S. Hyodo, *J. Comput. Appl. Math.*, **149**, 101 (2002).
- [2] S. Hyodo, *Mol. Sim.*, **30**, 887 (2004).
- [3] T. Kinjo and S. Hyodo, paper presented at the 1st NAREGI international conference, 1P52, Nara, Japan, 14-18 June (2005).
- [4] N. G. van Kampen and I. Oppenheim, *Physica*, **138A**, 231 (1986).
- [5] R. L. C. Akkermans and W. J. Briels, *J. Chem. Phys.*, **113**, 6409 (2000).
- [6] P. Espanol, *Phys. Rev. E*, **53**, 1572 (1996).
- [7] D. Cubero and S. N. Yaliraki, *J. Chem. Phys.*, **122**, 034108 (2005).
- [8] H. C. Allen, Jr., and P. C. Cross, *Molecular Vib-rotors*, John Wiley, New York, 1963.

Multiscale Equilibration of Poly (ethylene terephthalate) Melt

Kazunori Kamio¹, Krzysztof Moorthi¹, Doros N. Theodorou²

¹Computational Science Department, Materials Science Laboratory,
Mitsui Chemicals, Inc., 580-32 Nagaura, Sodegaura City, Chiba 299-0265, Japan,
kazunori.kamio@mitsui-chem.co.jp and krzysztof.moorthi@mitsui-chem.co.jp;

²Department of Materials Science and Engineering, School of Chemical Engineering,
National Technical University of Athens, 9 Heron Polytechniou Street, Zografou
Campus, Athens GR 15780, Greece, doros@chemeng.ntua.gr

ABSTRACT

New methodology for the multiscale equilibration of chemically complex polymer melts has been proposed and verified by applying it to Poly(ethylene terephthalate) (PET) melt. The Iterative Boltzmann Inversion (IBI) [1] coarse-graining scheme has been applied to reduce the chemical complexity of the polymer. The resulting structurally simpler model faithfully retains the original interactions. This facilitates the process of generalizing connectivity-altering Monte Carlo (MC) method, which has been used to equilibrate the Coarse-Grained (CG) PET model. The coarse-graining employed also reduces the number of degrees of freedom (d.o.f) in the system, which accelerates the calculations. The resulting method permits for thorough, multiscale equilibration of a 100-mer PET melt, and is applicable to a wide range of industrially important polymers. The CG melt density, characteristic ratio and other conformational properties agree with experiment. Topological analyses of the melt using CReTA [2] and Z [3] algorithms reveal that the melt is also well equilibrated with respect to entanglement density.

1. Introduction

PET-based resins are used for manufacturing fibers, films, drink bottles and replacements for commodity metals. Although a large number of experimental studies addressing structural, dynamic and barrier properties of PET is available, computational studies are scarce.

Due to the multiscale nature of polymeric systems, their physical properties often depend on several length scales. Therefore, in order to extract meaningful properties from molecular simulations, the systems must be equilibrated at all length scales relevant to the problem.

Pant and Theodorou developed an End Bridging Monte Carlo (EBMC) [4], which enabled drastic changes of chain connectivity in continuum MC simulations in a thermodynamically consistent fashion. Extensions of the method [5] have been effective in equilibrating highly entangled melts of linear and branched polyethylene (PE) as well as polypropylene, polydienes and polyethylene oxide.

In order to adapt EBMC methods to a wide range of polymers with complicated chemical structures, of which PET is an example, we coarse-grain PET chains using IBI methodology.

By testing the scaling properties of Kuhn lengths of subchains as proposed by Auhl et al [6], we find that the resulting method thoroughly equilibrates a melt composed of 100-mer PET chains at all length scales. The CG melt density, characteristic ratio and other conformational properties agree well with experiment. Topological analyses of the melt using the CReTA and Z algorithms reveal that the melt is also well equilibrated with respect to entanglement density.

2. Methods

2.1 Development of Coarse-Grained PET model

Fig. 1 presents the mapping scheme for coarse-graining of one repeat unit of PET. The proposed CG scheme reduces the number of d.o.f. per repeat unit, from 42 (united atom) to 9.

The CG interaction potentials for PET have been calculated on the basis of the atomistic model using the IBI Method. The molecular dynamics (MD) simulations of the ethylene terephthalate dimer system have been undertaken in order to derive the CG interaction potentials. The IBI Method was effective in optimizing the intra- and intermolecular potentials and distributions obtained from the atomistic MD simulations have been reproduced in the CG MD simulations.

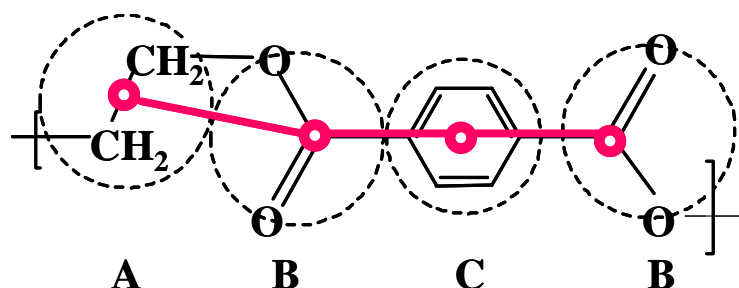


Figure 1. Schematic representation of the mapping scheme for CG PET.

2.2 Coarse-Grained Polymer Equilibration

The EBMC program developed by Pant and Theodorou [4] and Mavrantzas et al. [7] has been generalized here to handle linear polymers containing three bead types arranged in the $(\text{ABC})_n\text{A}$ sequence. Variable bond lengths have been implemented in MC moves. The EB move has been extended to enforce connectivity changes between monomers ABCB (Fig. 2).

A system containing ten 100-mer (19230g/mol) random coils, with density 1.25 g/cm^3 has been generated. The initial configurations contained many overlaps, which have been gradually eliminated by employing the EBMC method at constant volume. Next, in order to accelerate the volume equilibration, the system has been subjected to 1 ns of CG MD in the NpT ensemble. During this pre-equilibration process the average densities have converged to $1.23 \pm 0.01 \text{ g/cm}^3$. From this run six snapshots have been selected as starting configuration for the long EBMC runs.

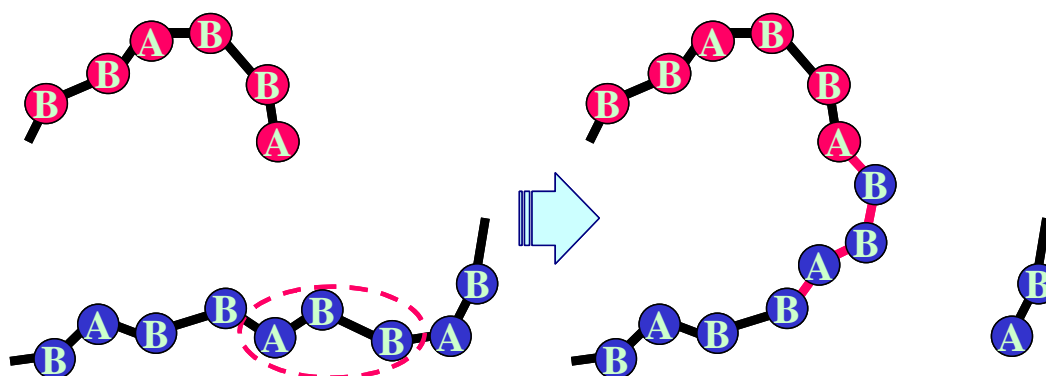


Figure 2. Schematic representation of EB move for PET chain.

3. Results and Discussion

3.1 Chain Conformation

Since small departures from equilibrium of the larger length scale features of chain conformations bring about only very small increase in free energy, the equilibration times of these features can be very long. Auhl et al. [6] characterize the equilibration of chain features within Kuhn and end-to-end length scales by the following Kuhn length-like quantity, $l_K(N)$,

$$l_K(N) = \frac{\langle R^2(N) \rangle}{\sum_{i=1}^n l_i} \propto \frac{\langle R^2(m) \rangle}{m} \quad (1)$$

where $R(N)$ is the end-to-end distance of a subchain containing N beads and l_i is the bond length between beads $i-1$ and i . For well-equilibrated chains $l_K(N)$ increases monotonically with the subchain length and asymptotically reaches the chain characteristic ratio, C_∞ , times the mean bond length along the contour. The quantity $\langle R^2(m) \rangle/m$, where m is the number of repeat units in the subchain, exhibits the same properties as $l_K(N)$. Fig. 3 presents $\langle R^2(m) \rangle/m$ as a function of m for combined data of six independent runs. The characteristic ratio of subchains increases monotonically with the subchain length within the range $1 < m < 15$. For $15 \leq m \leq 100$, it reaches a plateau whose value $140 \pm 0.5 \text{ \AA}^2$ corresponds to $\langle R^2 \rangle/M_w = 0.68 \pm 0.002 \text{ \AA}^2 \text{ g}^{-1} \text{ mol}$. The latter value is in very good agreement with the values derived on the basis of small-angle neutron scattering (SANS) measurements of PET melts. These results indicate that excellent equilibration of all PET chain conformations for $m \leq 100$ has been obtained.

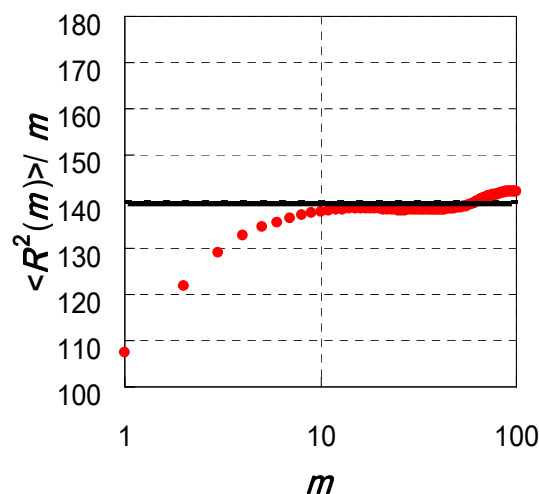


Figure 3. $\langle R^2(m) \rangle/m$ for PET subchains as function of the number of repeat units in the subchain, m . The line corresponds to the experimental value of $\langle R^2 \rangle/M_w = 0.69 \text{ \AA}^2 \text{ mol/g}$.

3.2 Entanglements in PET Melt

The statistical analysis of topological constraints in the PET melt has been performed using programs CReTA and Z. Primitive paths in the CG PET melt contain a large number of kinks, indicative of topological constraints due to chain uncrossability. The N_e values, averaged over 800 snapshots from a single MC run of length 800 million steps, using CReTA (31.8) and Z (35.8) algorithms, agree well with those obtained applying tube theory to rheological data for the plateau modulus, $N_e = 24-30$. Also, the tube diameter, d , 33.5 \AA (CReTA) and 35.8 (Z), obtained computationally as the Kuhn length of the primitive path, is in excellent agreement

with the literature value ($d=35$ Å). Next, Z algorithm has been applied to the analysis of the statistical properties of primitive path networks in all six MC runs. No significant differences in results from one and six runs are observed. These results indicate that very good equilibration of the melt topological structure has been achieved, as implied by the analysis of subchain Kuhn lengths.

4. Conclusions

A new method for the thorough, multiscale equilibration of chemically complex polymer melts has been proposed and verified by applying it to PET melt. First, the polymer structure is simplified by applying the IBI coarse-graining scheme. Next, the resulting coarse-grained polymer is equilibrated by connectivity altering MC scheme. The coarse-grained PET model accurately represents interactions of the atomistic original. Because of the generality of both schemes, the resulting method is applicable to a wide range of industrially important polymers.

The analysis of the subchain Kuhn length indicates that the PET melt is adequately equilibrated within Kuhn and chain length scales. Also, very good conservation of potential energy and averaged end-to-end distance is observed during the simulation. Consequently, excellent equilibration at the level of topological constraints has been achieved as evidenced by highly consistent values of interentanglement spacings in all MC runs. All MC runs produce highly consistent end-to-end distances and densities, which agree well with experiment.

Acknowledgements

We thank Dr. L. Peristeras for the solver of the EBMC code, Dr. Ch. Tzoumanekas for the results of CReTA calculations and the reprint of his paper prior publishing, and Prof. M. Kröger, Prof. V. Mavrantzas and Ms. K. Foteinopoulou for the reprint of their paper prior publishing and helpful comments on the Z code.

References

- [1] Coarse-Graining in Polymer Simulation: From the Atomistic to the Mesoscopic Scale and Back, F. Müller-Plathe, *Chem. Phys. Chem.* **3**, 754 (2002).
- [2] Topological Analysis of Linear Polymer Melts: A Statistical Approach, Ch. Tzoumanekas and D. N. Theodorou, *Macromolecules* **39**, 4592 (2006).
- [3] Shortest multiple disconnected path for the analysis of entanglements in two- and three-dimensional polymeric systems, M. Kröger, *Comp. Phys. Comm.*, **168**, 209 (2005).
- [4] Variable Connectivity Method for the Atomistic Monte Carlo Simulation of Polydisperse Polymer Melts, P. V. K. Pant and D. N. Theodorou, *Macromolecules* **28**, 7224 (1995).
- [5] Variable-Connectivity Monte Carlo Algorithms for Atomistic Simulation of Long-Chain Polymer System, D. N. Theodorou, in *Bridging Time Scales: Molecular Simulations for the next Decade*, edited by P. Nielaba, M Mareschal, and G. Ciccotti (Springer, Heidelberg, 2002)
- [6] Equilibration of long chain polymer melts in computer simulations, R. Auhl, R. Everaers, G. S. Grest, K. Kremer, and S. J. Plimpton, *J. Chem. Phys.* **119**, 12718 (2003).
- [7] End-Bridging Monte Carlo: A Fast Algorithm for Atomistic Simulation of Condensed Phases of Long Polymer Chains, V. G. Mavrantzas, T. D. Boone, E. Zervopoulou, and D. N. Theodorou, *Macromolecules* **32**, 5072 (1999).

Effects of hydrodynamic coherence on DNA translocation: a Lattice Boltzmann-Molecular Dynamics multiscale approach

Efthimios Kaxiras

Harvard University, Lyman Laboratory - Department of Physics, 02138 Cambridge, USA

We have developed a multi-scale approach to the modeling of long biomolecule dynamics in the presence of a fluid solvent, which combines Molecular-Langevin-Dynamics techniques with a mesoscopic Lattice-Boltzmann (LB) method for the solvent dynamics. A unique feature of the present approach is that hydrodynamic interactions between the solute biomolecules and the aqueous solvent are handled explicitly, and yet in a computationally tractable way due to the dual particle-field nature of the lattice Boltzmann solver. The suitability of the present LB-MD multiscale approach is demonstrated for the problem of DNA fast translocation across a nanopore. It is found that hydrodynamic interactions result in a significant acceleration of the DNA translocation process.

Statistics in entangled polymers from primitive chain network simulations

Yuichi Masubuchi^{1,2}, Giovanni Ianniruberto³, Francesco Greco⁴ and Giuseppe Marrucci³

¹Department of Organic and Polymer Materials Chemistry, Tokyo University of Agriculture and Technology, ²Japan Science and Technology, Tokyo 184-8588, Japan;

³Dipartimento di Ingegneria Chimica, Università degli studi di Napoli "Federico II",

⁴Istituto per i Materiali Compositi e Biomedici – CNR,
Piazzale Tecchio 80-80125 Napoli, Italy

ABSTRACT

Equilibrium distributions of entanglement spacing and number of entanglements per chain, and radial distribution of entanglement nodes are here investigated through primitive chain network simulations. Primitive chains are dispersed and connected in real space, and then equilibrated by force balance at entanglements, inclusive of osmotic forces due to density fluctuations. All known relaxation mechanisms such as reptation, contour length fluctuation, and constraint release are automatically accounted for in the simulation. It is shown that i) the length distribution of the entanglement spacing and the distribution of entanglement number per chain are consistent with theoretical predictions [J. D. Schieber, *J. Chem. Phys.*, 118, 5162 (2003)], and that ii) the radial distribution function for the entanglement network reveals a local condensation of the nodes, consistently with atomistic simulations [C. Tzoumanekas and D. N. Theodorou, *Macromolecules*, 39, 4592 (2006)]. The molecular weight corresponding to the mesh spacing of the simulated entanglement network is also discussed, by comparison with rheological data available in the literature.

1. Introduction

Though it has been established that the reptation picture can well explain entangled polymer dynamics [1], definition of entanglements is still under discussion. Recently, microscopic simulations [2-4] have offered valuable insights for bridging the microscopic description and the reptation-based description of the polymeric network. Multi-scale calculations combining the microscopic simulations with the models based on the reptation or sliplink [5,6] pictures appears then to be within reach. However, it has not yet been established how the microscopically obtained structure can be mapped onto the primitive chains employed in the reptation or sliplink pictures, since 3D structure of the entangled network has never been considered in the conventional entanglement based pictures [5]. In this study, we investigate entanglement network properties within the primitive chain network model [6], where many chains are dispersed in the simulation box (similarly to the molecular dynamics simulations) and dynamics of the entanglement points is ruled by force balances also accounting for the osmotic force due to the inter-chain interactions.

2. Model and Simulation

Polymers are replaced by consecutive segments which stand for elemental strands of the entanglement network. Based on the sliplink picture of entanglements, monomers can be exchanged between adjacent segments along the polymer. Differently from other sliplink models [5], the segments are also inter-molecularly connected in 3D space. Diffusion of

polymers is achieved by rearrangement of the interchain connections, which occurs when a chain end vacates or creates a sliplink. For the 3D sliplink motion and the monomer transport through sliplinks, i) elastic forces in each strand, ii) osmotic force due to chemical potential gradient, iii) drag force, and iv) thermal agitation are considered in the model. In the simulations we choose the average strand length a as the unit length and its Rouse relaxation time as the unit time. Usual periodic boundary conditions are employed, and the box size is 12^3 . The average number density of segments in space is fixed at 10.

3. Results and Discussion

Fig.1 shows the equilibrium statistics of an entanglement network, with chains made up of 10 segments (on average). The distribution of the number Z of segments per chain is consistent with a Poissonian distribution (Fig. 1a), and the segment-length distribution clearly shows an exponential tail. These results are consistent with Schieber's theoretical prediction [7], and with microscopic simulations [3,4].

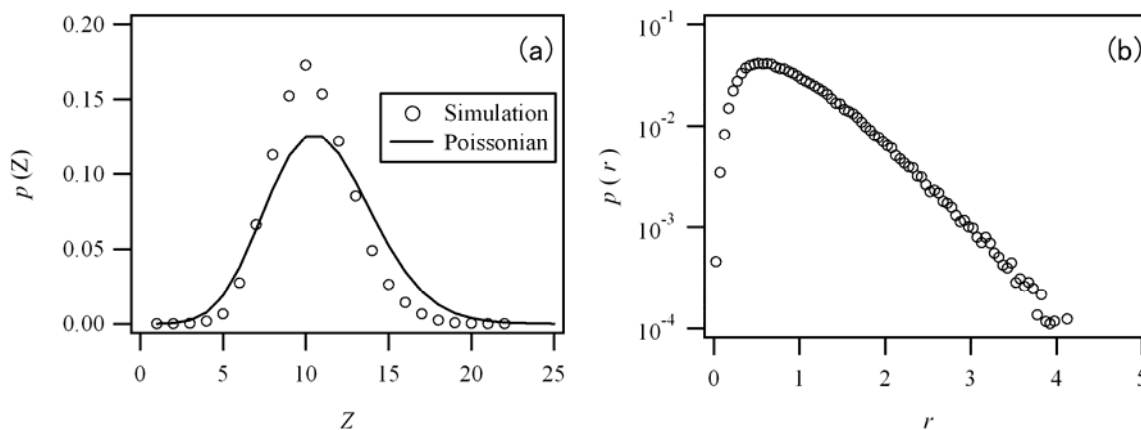


Figure 1. Distribution of (a) number of the segments per chain and (b) segment lengths.

Fig.2 shows radial distribution of the entanglement nodes, where directly connected consecutive nodes are not counted. An accretion of the nodes below $0.5a$ is observed, reflecting a local clustering. This result also is consistent with very recent atomistic simulations [8].

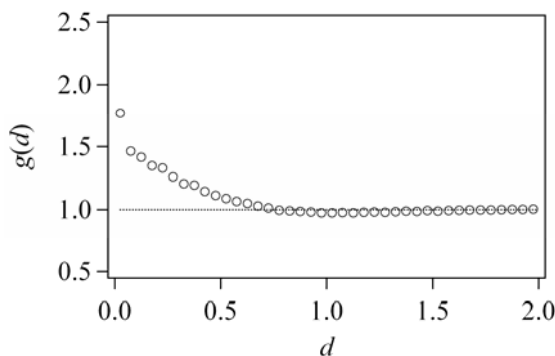


Figure 2. Radial distribution of entanglement nodes.

Fig.3 shows model predictions of linear viscoelasticity of several monodisperse polymer melts. It should be noted that the entanglement molecular weight coming out from our

simulations ($M/\langle Z \rangle$ in Fig. 3) is 60-70% of the tabulated entanglement molecular weight in the literature. The reason for this is node fluctuation in 3D space [9], which is not considered in standard models [1], whereas it is automatically included in our simulations.

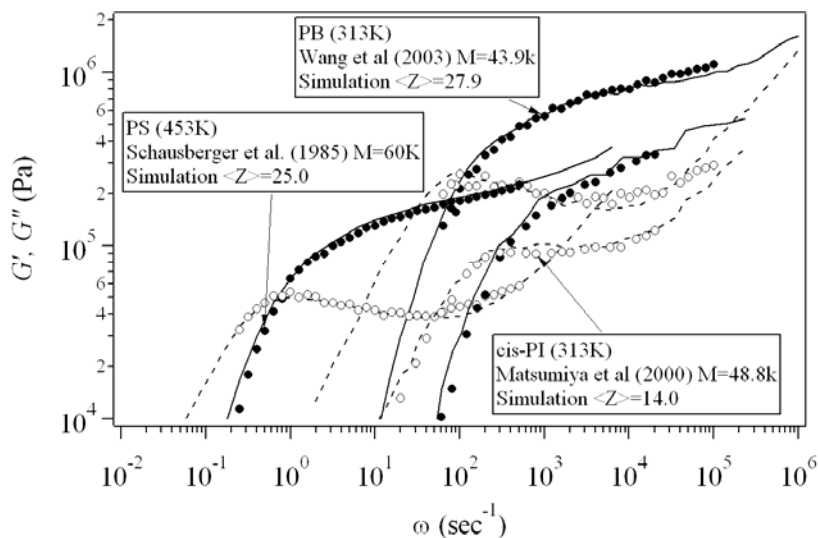


Figure 3. Prediction of linear viscoelasticity for several polymers.

Acknowledgements

This study was partly supported by Grants in Aid for Scientific Research [KAKENHI] 2006 from the Ministry of Education, Culture, Sports, Science and Technology of Japan.

References

- [1] M. Doi and S. F. Edwards, *The Theory of Polymer Dynamics* (Clarendon, Oxford, 1986)
- [2] R. Everaers, S. K. Sukumaran, G. S. Grest, C. Svaneborg, A. Sivasubramanian, and K. Kremer, *Science* 303, 823 (2004).
- [3] S. Shanbhag and R. G. Larson, *Macromolecules* 39, 2413 (2006).
- [4] K. Foteinopoulou, N. Ch. Karayiannis, V. G. Mavrantzas and M. Kröger, *Macromolecules*, 39, 4207 (2006).
- [5] C. C. Hua and J. Schieber, *J. Chem. Phys.* 109, 10018 (2001).
- [6] Y. Masubuchi, J. Takimoto, K. Koyama, G. Ianniruberto, F. Greco and G. Marrucci, *J. Chem. Phys.*, 115, 4387 (2001).
- [7] J. D. Schieber, *J. Chem. Phys.*, 118, 5162 (2003).
- [8] C. Tzoumanekas and D. N. Theodorou, *Macromolecules*, 39, 4592 (2006).
- [9] Y. Masubuchi, G. Ianniruberto, F. Greco and G. Marrucci, *J. Chem. Phys.*, 119, 6925 (2003).

Challenges in Polymer Simulation

Florian Mueller-Plathe

Physikalische Chemie, TU Darmstadt, Petersenstr. 20, 64287 Darmstadt, Germany

Systematic coarse-graining procedures for polymer models have opened the way to new applications of simulation to real polymeric systems. These procedures work for polymers both in the bulk and in solution, and they reproduce structural distributions as well as some thermodynamic properties. Future challenges lie in the correct prediction of dynamical and mechanical properties and in closing more of the length-scale and time-scale gaps between established models and simulation techniques.

Modeling the polymer-precursor synthesis of the amorphous ceramic α - $\text{Si}_3\text{B}_3\text{N}_7$ via a separation of time scale stepping stone approach

J. C. Schön¹, A. Hannemann², M. Jansen³

Max-Planck-Institute for Solid State Research, Heisenbergstr. 1, D-70569 Stuttgart, Germany;

e-mail: ¹C.Schoen@fkf.mpg.de, ²A.Hannemann@fkf.mpg.de, ³M.Jansen@fkf.mpg.de

ABSTRACT

The polymer-precursor synthesis of the amorphous ceramic α - $\text{Si}_3\text{B}_3\text{N}_7$ is modeled via a separation of time scale stepping stone approach. The resulting model is in good agreement with experimental measurements, in contrast to models based on quenching a $\text{Si}_3\text{B}_3\text{N}_7$ melt.

1. Introduction and Modeling Procedure

$\text{Si}_3\text{B}_3\text{N}_7$ is the parent compound of a new class of amorphous ceramics constituted of silicon, boron, nitrogen, and carbon, featuring a set of properties that is without precedent, and represents a prototypical random network based on chemical bonds of predominantly covalent character.[1,2] In contrast to many other amorphous materials of technological interest, α - $\text{Si}_3\text{B}_3\text{N}_7$ is not produced via glass formation, i.e. by quenching from a melt, the reason being that the binary components, BN and Si_3N_4 , melt incongruently under standard conditions. Neither has it been possible to employ sintering of μm -size powders consisting of binary nitrides BN and Si_3N_4 . Instead, one employs the so-called sol-gel route starting from single component precursors such as TADB ($(\text{SiCl}_3)(\text{NH})(\text{BCl}_2)$). In order to determine the atomic structure of this material, it has proven to be necessary, to simulate the actual synthesis route.[2,3]

Since the complete polymer-precursor route extends over many time and length scales, we have developed a stepping stone approach in order to simulate the synthesis as faithfully as possible.[4,5] Initially, precursor molecules are in solution with an excess of NH_3 , which react with each other based on the number of available reactive sites per molecule and their density within the solution. During this first linking stage, we take the likelihood that a given reaction attempt is successful to depend on whether a Si-N or a B-N bond is formed, with B-N bonds being energetically preferred. The diffusion rates of the individual molecules being relatively high, local depletion effects in the precursor-concentration do not play a big role and thus the precursor density can be taken to be spatially homogeneous. The first reaction stage can therefore be modeled by generating lists of linked precursor molecules ($n_{\text{TADB}} < 10$) according to these probabilities.

However, once several precursor molecules have linked up to form a larger aggregate, this oligomer will move much more slowly compared to the remaining original precursor and NH_3 molecules. Thus, the oligomers will become essentially stationary and serve as condensation centers for the still mobile reactants. This allows us to model this latter phase of the synthesis as a multiple condensation process of individual oligomers and monomers. At

the end of this stage, we are left with many isolated oligomers, which are now beginning to cross-link to form the polymer stage. This is modeled by placing the oligomers randomly on a lattice and shrinking the average distance until they can interact and form bonds. Finally, the pyrolysis stage is simulated by a Monte Carlo simulation at $T = 1200$ K, which stays well below the melting temperature ($T_{\text{melt}}(\text{Si}_3\text{B}_3\text{N}_7^{\text{cryst}}) \approx 2500$ K and $T_{\text{melt}}(\text{Si}_3\text{B}_3\text{N}_7^{\text{amorph}}) \approx 2000$ K) of the system but nevertheless eliminates most of the many dangling bonds still present in the polymer. During the pyrolysis simulations, the density of the polymer increases from $\rho \approx 1.5 \text{ g/cm}^3$ to the final value of $\rho_E = 1.8 - 2.0 \text{ g/cm}^3$.

2. Results and Discussion

Fig.1 shows a comparison of two models of $\text{Si}_3\text{B}_3\text{N}_7$, where model A (Fig. 1, left) has been generated by quenching a melt of $\text{Si}_3\text{B}_3\text{N}_7$,[3] and model E (Fig. 1, right) is the result of reproducing the precursor route,[4,5] respectively (notation according to ref. 3). One clearly recognizes that model E exhibits an inhomogeneous distribution of the cations, Si and B, within the random network on a sub-nanometer scale, while model A follows Löwenstein's rule and shows a perfectly homogeneous cation distribution. NMR-experiments confirm that the actual ceramic also possesses such a cation clustering,[2] while ESI-studies (electron spectroscopy imaging) show that such cation clusters do not exceed a size of 1 – 2 nm.[2] Another important quantity, which is correctly reproduced by model E is the density of the ceramic, $\rho_{\text{exp}} \approx 1.9 \text{ g/cm}^3$ [2], in contrast to $\rho_A = 2.6 - 2.9 \text{ g/cm}^3$ for model A. Finally, the experimental pair correlation functions measured with neutron and X-ray scattering are in better agreement with the ones calculated for model E than with those of model A.[3]

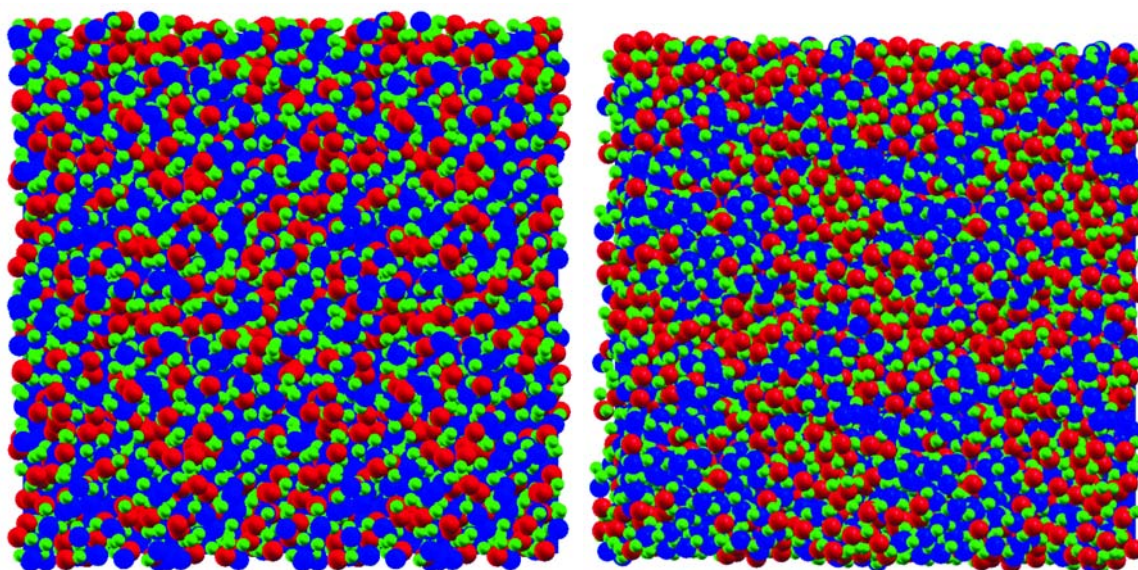


Figure 1 : Structure models of $\text{a-Si}_3\text{B}_3\text{N}_7$ generated by quenching from the melt (A, left) and by following the precursor-route (E, right). Si: red balls; B: blue balls; N: green balls.

Analyzing the structure of the precursor-derived model shows that the low density of the ceramics is due to the formation of sub-nanometer size voids during the linking of the small oligomers to the full polymer, which have not vanished during the pyrolysis. On the other hand, our simulations of the quench from the melt show that these voids would not be present if the material had been heated up to the melting point (c.f. Fig. 2). In order to investigate the

stability of the voids during the pyrolysis process in more detail, we have performed long-time simulations of distributions of large ($R_{\text{void}} = 0.8$ nm) and small ($R_{\text{void}} = 0.3$ nm) voids at temperatures ranging from 300 – 1500 K.[6] We find that the density of the ceramics increases very slowly (logarithmically) with time, with large voids surviving up to 1500 K.

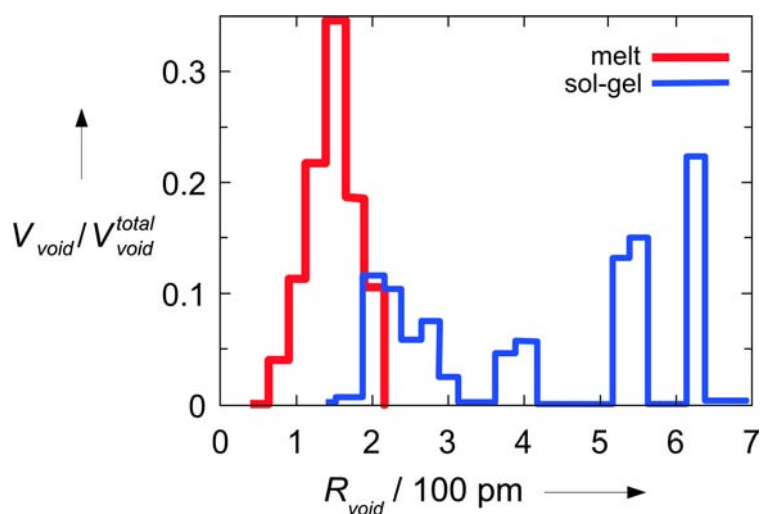


Figure 2: Distribution of voids of radii R_{void} for models of $\alpha\text{-Si}_3\text{B}_3\text{N}_7$ generated by quenching from the melt (red) and following the sol-gel precursor route (blue), expressed in terms of the void volume normalized to the total volume of all voids in the model.

Following the actual synthesis route in the computer allows us to judge the effects of various process parameters on the final product.[4,5] One particular point of interest is the cause of the inhomogeneous cation distribution in the ceramic, because energetically the homogeneous ceramics are lower than the inhomogeneous ones. Our investigations show that the decisive influence is the difference in reaction probability when forming a B-N vs. a Si-N bond. Similarly, the average size of the voids and their size distribution depends to some extent on the size of the oligomers at the moment when they start inter-linking.

References

- [1] M. Jansen, and P. Baldus, “Novel High-Performance Ceramics: Amorphous Inorganic Networks from Molecular Precursors”, *Angew. Chem. Int. Ed.* **36**, 328 (1997).
- [2] M. Jansen, J. C. Schön, and L. v. Wüllen, “The Route to the Structure Determination of Amorphous Solids: A Case Study of the Ceramic $\text{Si}_3\text{B}_3\text{N}_7$ ”, *Angew. Chem. Int. Ed.* **45**, 4244 (2006).
- [3] A. Hannemann, J. C. Schön, H. Putz, T. Lengauer, and M. Jansen, “Modeling amorphous $\text{Si}_3\text{B}_3\text{N}_7$: Structure and elastic properties”, *Phys. Rev. B* **70**, 144201 (2004).
- [4] J. C. Schön, A. Hannemann, and M. Jansen, “Modeling the Synthesis of Amorphous $\text{Si}_3\text{B}_3\text{N}_7$ via a Sequence of Dynamically Well-Separated Steps”, *J. Phys. Chem. B* **108**, 2210 (2004).
- [5] A. Hannemann, J. C. Schön, and M. Jansen, “Modeling the sol-gel synthesis route of amorphous $\text{Si}_3\text{B}_3\text{N}_7$ ”, *J. Mater. Chem.* **15**, 1167 (2005).
- [6] A. Hannemann, J. C. Schön, and M. Jansen, “Stability of nanovoids in amorphous $\text{Si}_3\text{B}_3\text{N}_7$ ”, *Phil. Mag.* **85**, 2621 (2005).

Hierarchical Modelling of Polymer Physical Properties

Doros N. Theodorou

School of Chemical Engineering, National Technical University of Athens, 9 Heroon Polytechniou Street, Zografou Campus, 157 80 Athens, Greece, doros@central.ntua.gr

ABSTRACT

The broad spectra of length and time scales governing the properties of real-life polymeric materials necessitate the development of hierarchical analysis and simulation methods for the successful prediction of these properties. We discuss some examples aimed at overcoming the challenges of long length and time scales in polymer simulations. The first example concerns the prediction of volumetric, thermal, and conformational properties of long-chain polymer melts. A new class of connectivity-altering Monte Carlo (MC) algorithms affords rapid equilibration of atomistic or coarse-grained models at all length scales. Direct topological analysis of the fully equilibrated melt configurations provides a tangible picture of entanglements. As a second example we discuss properties in the configurationally arrested glassy state. An energy landscape approach, wherein the polymer configuration is envisioned as fluctuating in the vicinity of local minima of the potential energy which depend on the spatial extent of the system, yields good estimates of the volumetric behaviour and elastic constants. Structural relaxation can be tracked as a sequence of transitions between neighbouring minima, whose rate constants are estimated via transition-state theory.

1. Equilibration and Entanglement Analysis of Long-Chain Polymer Melts

The full equilibration of detailed molecular models of long-chain polymer melts at all length scales has become possible through implementation of a class of connectivity-altering MC moves, such as end-bridging and double bridging, in combination with concerted rotation and reptation moves [1]. Connectivity-altering MC has been successfully applied to united-atom models of linear and long-chain branched polyethylene, polypropylene, cis-1,4 and 1,2-polybutadiene, cis-1,4 and trans-1,4 polyisoprene, and poly(ethylene oxide). For polymers of more complex chemical constitution, possessing large, inflexible moieties, a good strategy for equilibration is to first coarse-grain the atomistic model into a model involving many fewer degrees of freedom [2], equilibrate at the coarse-grained level using connectivity-altering moves, and then reverse-map to the atomistic level. Recently, this strategy has been applied to poly(ethylene terephthalate) (PET) [3]. The original atomistic model has been reduced to a coarse-grained model with only nine degrees of freedom per repeat unit, using the Iterative Boltzmann Inversion method of Müller-Plathe et al. [4]. Connectivity-altering simulations of a PET melt of mean degree of polymerization 100 at 450 K and 1 atm yielded excellent equilibration at all length scales. The mass density ρ of runs initiated at widely different configurations converged to a common value within 1% of experiment, and the ratio $\langle R^2 \rangle / M$ of mean squared end-to-end distance to molar mass was $0.68 \text{ \AA}^2 / (\text{g mol}^{-1})$, in good agreement with the range $0.61\text{-}0.69 \text{ \AA}^2 / (\text{g mol}^{-1})$ from small angle neutron scattering.

Well-equilibrated atomistic or coarse-grained configurations from connectivity-altering Monte Carlo serve as excellent starting points for long molecular dynamics (MD) simulations aimed at the investigation of segmental and chain dynamics. Segmental mean squared displacements and chain self-diffusivities obtained from MD clearly show the crossover from Rouse to reptation (entangled) dynamics with increasing chain length. An alternative, and

computationally less expensive, route for the detection of entanglements is to subject the MC-sampled configurations to topological analysis. We have recently developed a Contour Reduction Topological Analysis (CReTA) algorithm for this purpose [5]. Keeping the chain ends fixed, the algorithm reduces the contour lengths of all chains in parallel by implementing linearizing moves around randomly chosen segments, subject to the condition that two chains can never cross each other. The chain diameters are reduced during the latter stages of the procedure, so that the original configuration is ultimately mapped onto a set of zig-zag lines (“primitive paths”) coming together at points of topological constraint (“entanglements”).

Table 1: Results of CReTA analysis. N , \bar{N}_{ES} , and N_e are counted in skeletal carbons for PE and PB and in chemical repeat units for PET. Experimental values are shown in parentheses.

	N	\bar{N}_{ES}	\bar{d}_{ES} (Å)	N_e	d (Å)	p (Å)
PE	500	28.3	14.0	75.1 (61.4)	38.4 (38.5)	1.53 (1.69)
PE	1000	29.1	14.1	74.1 (61.4)	36.6 (38.5)	1.65 (1.69)
PB	1000	80.9	18.7	178.7 (173.8)	42.3 (43.0)	2.59 (2.44)
PET	100	3.5	14.2	7.9 (6.1-7.6)	33.5 (38.0-35.0)	1.82 (1.77-1.99)

A wealth of statistical extracted from the CReTA process [5] is valuable in reconstructing entanglement networks for the mesoscopic simulation of the rheological properties of melts and of the large-deformation behaviour of solid polymers. Quantitative measures of the entanglement structure are presented in Tab. 1 for two polyethylene (PE), a polybutadiene (PB), and a PET melt. N is the mean chain length; d and N_e are the length and number of monomers, respectively, of a Kuhn segment of the primitive path; \bar{d}_{ES} and \bar{N}_{ES} are the mean distance and number of segments between successive entanglements; and $p=M/(\rho N_A \langle R^2 \rangle)$ is the packing length. Values of d and N_e from CReTA agree with entanglement tube diameters and molecular weights from measurements of the plateau modulus. The network mesh size, as reflected by \bar{d}_{ES} and \bar{N}_{ES} , is only 40% of the Kuhn length of the primitive path [5].

2. Volumetric properties, elastic constants, and structural relaxation in polymer glasses

Although significant advances have been achieved in modelling ageing and deformation of polymer glasses macroscopically, connecting these properties to the chemical constitution, formation and processing history of a glass is still a challenge, because of the extremely broad spectra of characteristic times governing molecular motion in the glassy state.

Progress in the simulation of physical ageing and deformation of glassy materials can be achieved based on the idea that the configuration of a glass is trapped in the vicinity of a local minimum of the energy (inherent structure [6]), undergoing infrequent transitions to neighbouring minima across free energy barriers that may vary widely in height. This “energy landscape” picture focusses on the determination of representative energy minima and of the transition paths leading from those to neighbouring minima in the multidimensional configuration space of the glass. Thermodynamic properties and elastic constants in the individual energy minima are estimated by invoking a quasiharmonic approximation for the energy, and the corresponding properties of the glass are obtained through arithmetic (“quenched”) averaging over all minima. Rate constants for transitions from a minimum to neighbouring minima are estimated using the principles of multidimensional transition-state theory [7] and the temporal evolution of the system, in the presence or absence of external stress, is tracked by Kinetic Monte Carlo (KMC) as a

succession of transitions between the minima. Such “quasi-MD” simulations can deal with arbitrarily slow transition rates and thus overcome the problems of “brute-force” MD.

Application of this approach to glassy atactic polystyrene (PS), using a united-atom model, has led to excellent predictions for its volumetric properties. Uniaxial tensile tests on PS based on the landscape approach yielded a Young’s modulus $E=3.9$ GPa and a Poisson ratio $\nu=0.35$, which compare well with $E=3.2-3.4$ GPa and $\nu=0.32$ reported experimentally.

Fig.1 displays the self-part of the intermediate scattering function of a Lennard-Jones (LJ) glass, as obtained through a quasi-MD simulation. This function, which can be obtained experimentally by incoherent quasielastic neutron scattering, characterizes structural relaxation in the glass. One can discern an initial “fast β ” decay, which is due to motion about an inherent structure and occasional fast transitions to close-lying neighbouring minima. Then, for several decades in time, S_s remains pretty much constant at a nonzero value (“nonergodicity parameter”). Finally, it drops along a long-time “ α relaxation” process involving a cascade of transitions which, in the depicted case, ultimately leads to crystallization of the glass. The appearance is strikingly similar to that of $S_s(q,t)$ of supercooled liquids obtained by MD at temperatures close to the glass temperature.

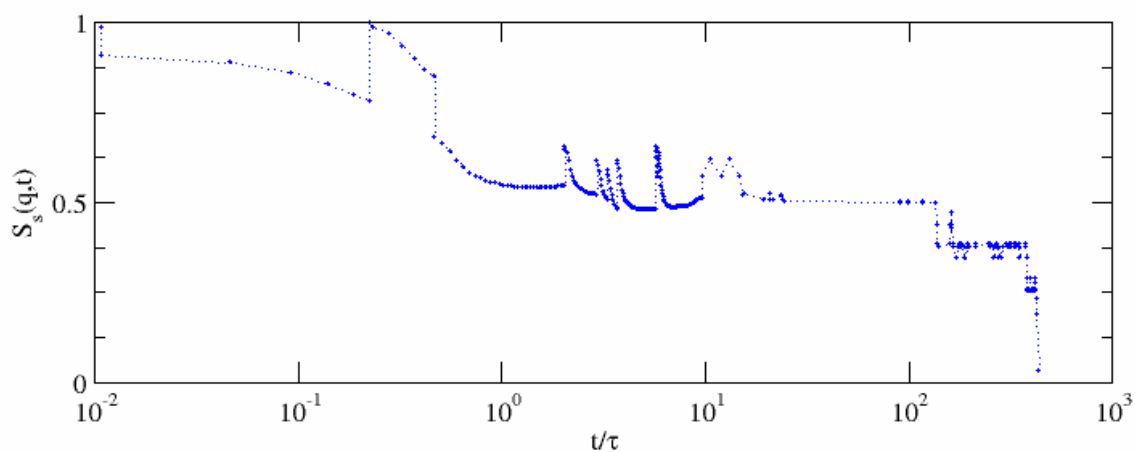


Figure 1. Self-part of the intermediate scattering function $S_s(q,t)$ from quasi-MD simulation of structural relaxation in a LJ glass at $P=1.003 \text{ } \epsilon/\sigma^3$ and $T=0.415 \text{ } \epsilon/k_B$. The glass was obtained by quenching from the melt at a rate $\dot{T}=-0.184 \text{ } \epsilon/(k_B \tau)$. $\tau=(m\sigma^2/\epsilon)^{1/2}$ is the LJ unit of time.

Acknowledgements

I am grateful to my collaborators Christos Tzoumanekas, George Boulougouris, Kazunori Kamio, Krzysztof Moorthi, Nikos Kopsias, Nikos Karayiannis, and Vlas Mavrantzas.

References

- [1] N.Ch. Karayiannis, V.G. Mavrantzas, D.N. Theodorou, D.N. *Phys. Rev. Lett.* **88**, 105502 (2002); D.N. Theodorou, in *Bridging Time Scales: Molecular Simulations for the Next Decade*, Eds. P. Nielaba, M. Mareschal, G. Ciccotti, (Springer-Verlag, Berlin, 2002), p. 69.
- [2] J. Baschnagel, K. Binder, P. Doruker, A. A. Gusev, O. Hahn, K. Kremer, W. L. Mattice, F. Müller-Plathe, M. Murat, W. Paul, S. Santos, U. W. Suter and V. Tries, *Adv. Polym. Sci.* **152**, 41 (2000).
- [3] K. Kamio, K. Moorthi, and D.N. Theodorou, *Macromolecules*, submitted.
- [4] D. Reith, M. Pütz, F. Müller-Plathe, *J. Comput. Chem.* **24**, 1624 (2003).
- [5] C. Tzoumanekas and D.N. Theodorou, *Macromolecules* **39**, 4592 (2006).
- [6] F.H. Stillinger, *Science* **267**, 1935 (1995).
- [7] N.P. Kopsias and D.N. Theodorou, *J. Chem. Phys.* **109**, 8573 (1998).

Mesoscopic Simulation of Micellar Structures in Amphiphilic Block Copolymer Solutions by the Density Functional Model

Author: Takashi Uneyama

Affiliation: Department of Physics, Graduate School of Science, Kyoto University
Kitashirakawa, Sakyo-ku, Kyoto 606-8502, JAPAN
uneyama@ton.sphys.kyoto-u.ac.jp

ABSTRACT

We performed mesoscopic dynamics simulation for micellar structures in amphiphilic diblock copolymer solution systems. We employed the free energy functional model for block copolymer blends and the stochastic dynamic density functional equation. Our simulation model reproduces micellar structure formation process from initial homogeneous state.

1. Introduction

The amphiphilic block copolymers form various interesting micellar structures such as spherical micelles, cylindrical micelles and vesicles in selective solvents [1].

The particle model simulations (for example, Brownian dynamics simulations [2] or dissipative particle dynamics simulations [3]) have been done to study the dynamics of micellar structure formations. For example, the following mechanism of vesicle formation from homogeneous state has been observed. First, small spherical micelles are formed rapidly. Next, the small micelles aggregate and form larger micelles (cylindrical micelles or disk like micelles). Finally the large disk like micelles close up spontaneously to form vesicles.

On the other hand, most of continuum model simulations are limited to equilibrium simulations [4,5]. Recently He and Schmid performed external potential dynamics simulations for vesicle formation process in block copolymer solutions [6], but their result does not agree with the results of particle simulations. This suggests that we need more improved continuum field model for dynamics simulations.

In this work, we propose the mesoscopic dynamics simulation model based on the density functional theory. Our model reproduces the micellar structure formation dynamics which is qualitatively same as the particle simulations.

2. Theory

AB diblock copolymer solutions can be modelled as AB diblock copolymer / S solvent blends. In the density functional theory, the free energy for the system is expressed as the functional of density fields of each components ($\phi_A(\mathbf{r})$, $\phi_B(\mathbf{r})$, and $\phi_S(\mathbf{r})$). In this work we use the following free energy functional [5] (for simplicity, we set $k_B T = 1$ hereafter).

$$\begin{aligned}
 F = & \sum_{i=(A,B)} \int d\mathbf{r} 2f_i C_{ii} \psi_i^2(\mathbf{r}) \ln \psi_i(\mathbf{r}) + \int d\mathbf{r} 2\psi_S^2(\mathbf{r}) \ln \psi_S(\mathbf{r}) \\
 & + \sum_{i,j=(A,B)} \int d\mathbf{r} d\mathbf{r}' 2\sqrt{f_i f_j} A_{ij} \tilde{\mathcal{G}}(\mathbf{r} - \mathbf{r}') \psi_i(\mathbf{r}) \psi_j(\mathbf{r}') \\
 & + \int d\mathbf{r} 4\sqrt{f_A f_B} C_{AB} \psi_A(\mathbf{r}) \psi_B(\mathbf{r}) + \sum_{i=(A,B,S)} \int d\mathbf{r} \frac{b^2}{6} |\nabla \psi_i(\mathbf{r})|^2 \\
 & + \sum_{i,j=(A,B,S)} \int d\mathbf{r} \frac{\chi_{ij}}{2} \psi_i^2(\mathbf{r}) \psi_j^2(\mathbf{r}) + \int d\mathbf{r} \frac{P(\mathbf{r})}{2} [\psi_A^2(\mathbf{r}) + \psi_B^2(\mathbf{r}) + \psi_S^2(\mathbf{r}) - 1]
 \end{aligned} \tag{1}$$

where $\psi_i(\mathbf{r}) \equiv \sqrt{\phi_i(\mathbf{r})}$, f_i is the block ratio of the i -subchain, b is the Kuhn length, and χ_{ij} is the Flory-Huggins χ parameter. A_{ij} and C_{ij} are constants determined from the architecture of the diblock copolymer. $\tilde{\mathcal{G}}(\mathbf{r} - \mathbf{r}')$ is the Green function which satisfies $[-\nabla^2 + \lambda^{-2}]\tilde{\mathcal{G}}(\mathbf{r} - \mathbf{r}') = \delta(\mathbf{r} - \mathbf{r}')$ (λ is the cutoff length for the interaction) [7]. $P(\mathbf{r})$ is the Lagrange multiplier which corresponds to the incompressible condition ($\phi_A(\mathbf{r}) + \phi_B(\mathbf{r}) + \phi_S(\mathbf{r}) = 1$).

It is emphasised that Eqn (1) is valid for strong segregation region at least qualitatively [5]. This is quite important because the vesicles are observed in the strong segregation region. To study various micellar structures, including vesicles, we need to use appropriate free energy functional.

We use the following stochastic dynamic density functional equation [8] for time evolution.

$$\frac{\partial \phi_i(\mathbf{r})}{\partial t} = \nabla \cdot \left[\frac{\phi_i(\mathbf{r})}{\zeta_i} \nabla \frac{\delta F}{\delta \phi_i(\mathbf{r})} \right] + \xi_i(\mathbf{r}, t) \quad (2)$$

where ζ_i is the friction coefficient of the i -monomer and $\xi_i(\mathbf{r}, t)$ is the Gaussian white noise which satisfies following relations.

$$\langle \xi_i(\mathbf{r}, t) \rangle = 0 \quad (3)$$

$$\langle \xi_i(\mathbf{r}, t) \xi_j(\mathbf{r}', t') \rangle = -2\tilde{\beta}^{-1} \delta_{ij} \nabla \cdot \left[\frac{\phi(\mathbf{r})}{\zeta_i} \nabla \delta(\mathbf{r} - \mathbf{r}') \right] \delta(t - t') \quad (4)$$

where $\tilde{\beta}^{-1}$ is the magnitude of the noise and is proportional to $k_B T (= 1)$. Here we emphasise that $\tilde{\beta}^{-1}$ is not equal to $k_B T$, but is determined from the characteristic (coarse-grained) time scale of $\phi_i(\mathbf{r})$ [8]. For simplicity we set $\zeta_i = 1/2$ hereafter. Eqn (2) can be rewritten as follows by using $\phi_i(\mathbf{r}) = \psi_i^2(\mathbf{r})$.

$$\frac{\partial \phi_i(\mathbf{r})}{\partial t} = \psi_i(\mathbf{r}) \nabla^2 \mu_i(\mathbf{r}) - \mu_i(\mathbf{r}) \nabla^2 \psi_i(\mathbf{r}) + \xi_i(\mathbf{r}, t) \quad (5)$$

where $\mu_i(\mathbf{r}) \equiv \delta F / \delta \psi_i(\mathbf{r})$ is the chemical potential with respect to $\psi_i(\mathbf{r})$. $\mu_i(\mathbf{r})$ can be calculated from $\psi_i(\mathbf{r})$ by using Eqn (1) (see also Ref [5]). The advantage of using Eqn (5) is that $\mu_i(\mathbf{r})$ does not have singularity at $\psi_i(\mathbf{r}) = 0$ where $\delta F / \delta \phi_i(\mathbf{r})$ has singularity at $\phi_i(\mathbf{r}) = 0$. Thus we can perform stable simulations for strong segregation systems.

3. Simulation

Simulations can be done by desecritizing Eqn (5) and solving it numerically. We employed partial implicit scheme to improve numerical stability [5].

Parameters were set as follows. The polymerization index of diblock copolymer $N = 10$, the block ratio $f_A = 1/3$, $f_B = 2/3$, the Kuhn length $b = 1$, the cutoff length for long range interaction $\lambda = 5$, the volume fraction of diblock copolymers $\bar{\phi}_p = 0.2$, Flory-Huggins χ parameters $\chi_{AB} = 2.5$, $\chi_{AS} = -0.5$, $\chi_{BS} = 5$ (The A subchain is hydrophilic and the B subchain is hydrophobic), and the magnitude of the noise $\tilde{\beta}^{-1} = 0.3125$. The initial state is homogeneous state ($\phi_A(\mathbf{r}) = f_A \bar{\phi}_p$, $\phi_B(\mathbf{r}) = f_B \bar{\phi}_p$, $\phi_S(\mathbf{r}) = 1 - \bar{\phi}_p$) and the boundary condition is the periodic boundary condition.

Simulations are carried out for two dimensional systems as well as the three dimensional systems. The snapshots of the simulation for the three dimensional system (system size 24^3 , lattice points 48^3 , time step $\Delta t = 0.0025$) is shown in Fig 1. We can observe the vesicle is formed from the homogeneous initial state. The vesicle formation mechanism is similar to the result of the particle simulations; At the initial stage, small micelles are formed rapidly. Then micelles grow by collision and coalescence process. At the late stage, the disk like micelle close up to form a vesicle. We also obtained various micellar structures by changing parameters such as $\bar{\phi}_p$ or χ_{BS} .

It is noted that at the late stage of micellar formation processes, the noise play an important role. As observed in Fig 1, the noise used in this simulation is large and micellar

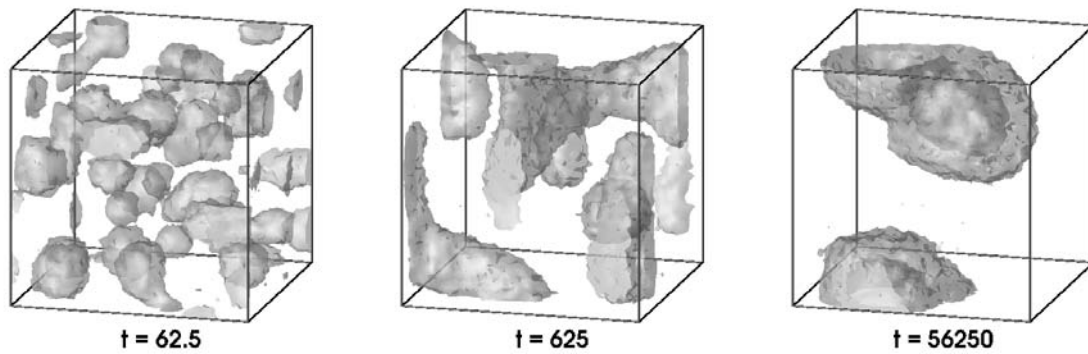


Figure 1: Snapshots of micellar structures in the amphiphilic diblock copolymer solution ($t = 62.5, 625, 56250$, from left to right). The grey surface is the isosurface for $\phi_B(\mathbf{r}) = 0.5$.

structures were fluctuating strongly. Without the effect of the noise, the Brownian motion of small spherical micelles cannot be observed, and thus no larger structures are formed.

4. Conclusion

We proposed the mesoscopic continuum model for dynamics simulations of micellar systems. We employed the free energy functional model (Eqn (1)) based on the density functional theory and the stochastic dynamic density functional equation (Eqn (5)). We carried the numerical simulations and found that our model reproduces the micellar formation dynamics which is consistent with the particle model simulations.

Acknowledgements

This work is supported by the Research Fellowships of the Japan Society for the Promotion of Science for Young Scientists. The author thanks H. Fursawa, T. Kawakatsu and T. Ohta for helpful comments and discussions.

References

- [1] A. Choucair and A. Eisenberg, *Eur. Phys. J. E* **10**, 37 (2003).
- [2] H. Noguchi and M. Takasu *Phys. Rev. E* **64**, 041913 (2001).
- [3] S. Yamamoto, Y. Maruyama and S. Hyodo, *J. Chem. Phys.* **116**, 5842 (2002).
- [4] X. He, H. Liang, L. Huang and C. Pan, *J. Phys. Chem. B* **108**, 1731 (2004).
- [5] T. Uneyama and M. Doi, *Macromolecules* **38**, 5817 (2005).
- [6] X. He and F. Schmid, *Macromolecules* **39**, 2654 (2006).
- [7] H. Tang and K. F. Freed, *J. Phys. Chem.* **97**, 4496 (1992).
- [8] A. J. Archer and M. Rauscher, *J. Phys. A: Math. Gen.* **37**, 9325 (2004).

The modeling and simulation of dot formation kinetics in the drying process of polymer solution drop

Tatsuya Yamaue, Youngki Jung and Masao Doi

**Department of Applied Physics, The University of Tokyo
Hongo 7-3-1, Bunkyo-ku, Tokyo 113-8656, Japan.**

ABSTRACT

A model based on both the Hu-Larson model for droplet flow and the stress-diffusion coupling model for gel dynamics is proposed for the drying process and stain formation of polymer solution droplets having mixed solvents of high volatile / low surface tension and low volatile / high surface tension. The model is analyzed theoretically and simulated by multi-physics techniques. Results show that the flux of solute from the center to edges of a droplet in the evaporation process has a minimum value at some mixing ratio of solvents, where a stain becomes a cap shape. The results reproduce experimentally observed ones, which are also described in this paper, for the drying process of polystyrene polymer solution drops about $100 \mu\text{m}$ radius having anisole / ethylacetate mixed solvents, whose evaporation rates are quite different, placed on a hydrophobic substrate.

1. Introduction

How to control the shape of the solute deposit in the drying process of a polymer solution drop on a substrate is an important problem in the ink-jet printing. In the case of dilute solution, a commonly observed phenomena is the "coffee stain" : the evaporation of solvent induces an outward flow and creates a ring-like deposit after drying. [1] The outward flow is a result of the combined action of the increased evaporation rate at the droplet edge, and contact line pinning caused by solute deposition near the edge (self-pinning). [2] De Gans et.al. showed that when a polymer solution is dried on a glass slide coated with hydrophobic materials, it leaves a small dot after the evaporation. [3] They observed that the dots have small dimple in the center, the size of which can be changed by solvent. They, however, did not conduct any quantitative study for the phenomena.

In the previous paper [4], we show that, when the solvent is pure anisole, the shape of the final polymer deposit changes from concave dot for dilute cases, to flat dot for 5wt% initial density case, and then to concave dot again in dense cases with the increase of the initial polymer concentration. This shape change is caused by the gradual transition from the solute piling mechanism proposed by Deegan et.al. to the crust buckling mechanism proposed by de Gennes and Pauchard. [5]

Here, we studied the shape change, flow and contact line motion in drying process of polystyrene polymer solution drops of 0.5wt% about $100 \mu\text{m}$ radius placed on a hydrophobic substrate having anisole/ethylacetate mixed solvents, where anisole is a low volatile and high surface tension solvent, ethylacetate is a high volatile and low surface tension solvent and these evaporation rates are quite different. A model based on both the Hu-Larson model [6] for droplet flow and the stress-diffusion coupling model for gel dynamics [7] is proposed for the drying process and stain formation of polymer solution droplets having mixed solvents of high volatile / low surface tension and low volatile / high surface tension. The model is

analyzed theoretically and simulated by multi-physics techniques of combining a flow model and a gel model.

2. Experiment

The drying process of polystyrene polymer solution 0.5wt% drops of various anisole/ethylacetate mixed solvents are observed experimentally, where the equilibrium contact angle for each solvent are 85 degree for anisole and 55 degree for ethylacetate. The drying process generally takes place in three stages. First, the droplet evaporates keeping the contact line fixed and the contact angle decrease. Second, when the contact angle reaches to a receding contact angle, the droplet starts to shrink with a receding contact angle. Finally the contact line pinned again by self-pinning, and the droplet starts to be deformed from a spherical cap shape. Fig.1 shows the time evolution of a droplet volume (Fig.1(a)) and a contact angle (Fig.1(b)) related to time. The evaporation rate becomes small as the anisole component becomes rich. In the anisole rich region, the evaporation becomes uniformly small, while in the ethylacetate rich region, the two step evaporations can be observed, where the evaporation rate changes drastically. The evaporation rates for pure anisole solution and pure ethylacetate solution are about $0.5\mu\text{m}/\text{sec}$ and $12\mu\text{m}/\text{sec}$. The receding contact angle becomes large as the anisole component becomes rich, where the receding contact angle for each solvent are 70 degree for anisole and 40 degree for ethylacetate. When the mixed ratio of ethylacetate is about 90%, both a ring-like deposit and a dot-like deposit in it can be observed together.

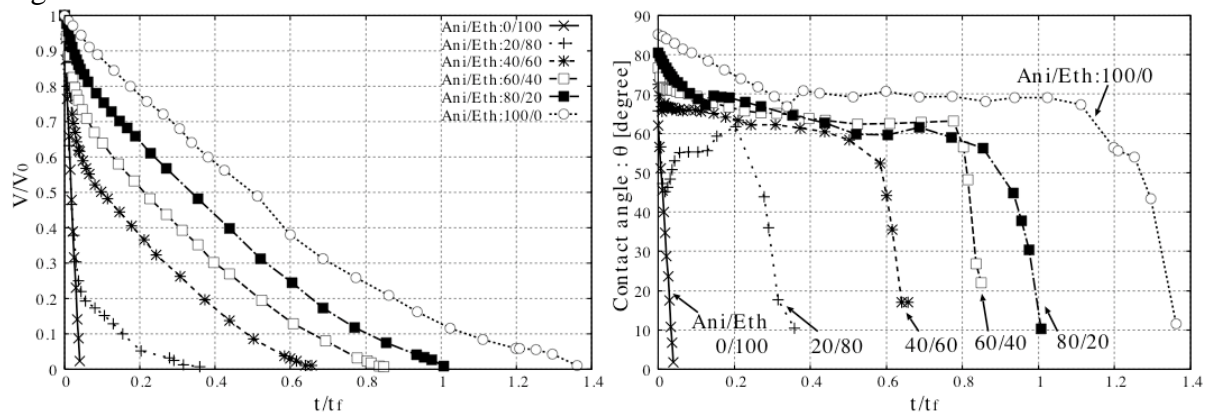


Fig.1 : The time evolution of a droplet volume ((a) left) and a contact angle ((b) right) related to time.

Fig.2(a) shows the height profile of a stain after evaporation. As the mixed ratio of ethylacetate increases from pure anisole in the initial density 0.5wt% case, the dimple of the final polymer deposit decreases, and the shape becomes flat, when anisole/ethylacetate mixing ratio is about 60%/40%. This change is considered to be caused by the temperature Marangoni flow induced by high volatile solvent component and the density Marangoni flow induced by the difference of surface tensions of mixed solvents. In the other hand, the mixed ratio of ethylacetate increases between 60% and 80%, the dimple of the final polymer deposit increases again. This change is considered to be caused by increasing of the outward flow induced by high volatile solvent. Fig.2(b) shows the averaged polymer volume fraction at the self-pinning time related to the mixed ratio of solvent. The averaged polymer volume fraction has a maximum value when the anisole ratio is about 60%, which almost agrees with one where the shape of dot becomes a cap-like shape. This means the flow field during the receding process before the self-pinning time is important to explain the difference of stain shapes.

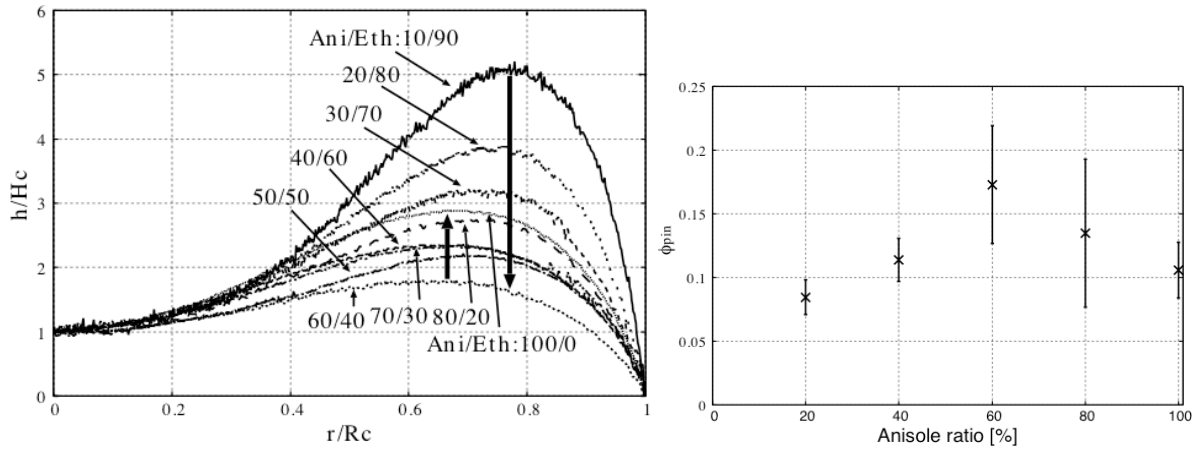


Fig.2 : The height profile of a stain after evaporation ((a) left) and an averaged polymer volume fraction at the self-pinning time related to the mixed ratio of solvent. ((b) right)

3. Theoretical Analysis and Simulation

We analyze and simulate the flow of polymer solute in the evaporation process of polymer solution drops using the competition model of the Marangoni flow and the outward flow, each model is based on the Hu-Larson model [6], and the shape change in the evaporation and gelation process after selfpinning using the stress diffusion coupling model of gel dynamics based on the two fluids model of polymer and solvent. [7]

According to the Hu-Larson model, the averaged pressure difference related to the outward flow ΔP_{out} between the center and edge of a droplet is described as follows.

$$\Delta P_{out} \cong -\frac{\eta}{\delta} J_{av} \lambda \left(\frac{R}{\delta} \right)^\lambda \quad (1)$$

$$\lambda(\theta) = \frac{1}{2} - \frac{\theta(C_{ani})}{\pi}$$

where η is viscosity, δ monomer size, R droplet radius, the contact angle θ is a function of the anisole ratio C_{ani} of mixed solvent. The averaged evaporation rate J_{av} is described by

$$J_{av} \cong C_{ani} J_{ani} + (1 - C_{ani}) J_{ety}. \quad (2)$$

where J_{ani} and J_{ety} are evaporation rates for anisole and ethylacetate. In the other hand, the averaged pressure difference related to the thermal Marangoni flow ΔP_{mar} between the center and edge of a droplet is described as follows.

$$\Delta P_{mar} \cong -\frac{d\gamma}{dr} \cong \frac{1}{R} \beta \Delta T \quad (3)$$

$$\Delta T \cong \frac{1}{k} L \rho R J_{ave}$$

where γ is surface tension which increases as the temperature T on surface decreases. ΔT is temperature difference between top of a droplet and the substrate, k the thermal conductivity, L the latent heat, and ρ is the mass density.

Fig.3 shows the pressure difference between the center and edge of a droplet related to the mixing ratio of solvent calculated by eqs.(1) and (3), where a dashed line and a dotted line describe the contribution of the outward flow and the Marangoni flow each other. Results show that the flux of solute from edge to the center of a droplet in the evaporation process has a maximum value at some mixing ratio of solvents, where a stain becomes a cap shape. The results reproduce experimentally observed ones.

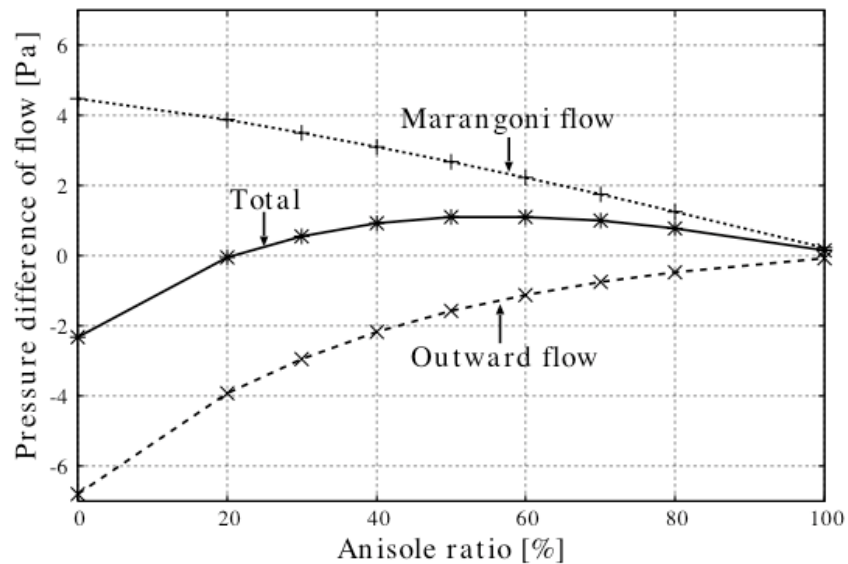


Fig.3 : Pressure difference between the center and edge of a droplet related to the mixing ratio of solvent, where a dashed line and a dotted line describe the contribution of the outward flow and the Marangoni flow each other.

These results are compared and discussed with the simulation results of the thermal Marangoni flow and the time evolution of solute distribution by the finite element method. Fig.3 shows the outward flow field during the evaporation process for droplets having 30 degree contact angle and 90 degree contact angle by FEM each other.

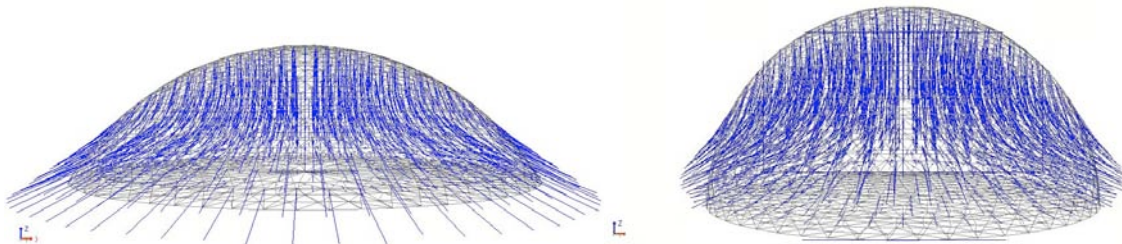


Fig.4 : Pressure difference in a droplet related to mixing ratio and flow field in evaporation process by FEM simulation.

Acknowledgements

This work is partially supported from NEDO (New Energy and Industrial Technology Development Organization), METI, Japan.

References

- [1] R. D. Deegan, et. al. : Nature 389, 827 (1997) : Phys. Rev. E62, 756 (2000) : Phys. Rev. E61, 475 (2000).
- [2] M. D. Haw, M. Gillie and W. C. Poon, Langmuir 18, 1620 (2002).
- [3] B. J. de Gans and U. S. Schubert : Langmuir 20, 7789 (2004).
- [4] L. Pauchard, et. al. : Europhys. Lett 62, 897 (2003) : Phys. Rev. E68, 052801 (2003) : Langmuir 20, 5138 (2004).
- [5] T. Kajiyama, E. Nishitani, T. Yamaue, M. Doi : Phys. Rev. E73, 11601 (2006).
- [6] H. Hu and R. G. Larson : Langmuir 21, 3963 (2005) : Langmuir 21, 3972 (2005).
- [7] T. Yamaue and M. Doi : Phys. Rev. E70, 011401 (2004) : J. Chem. Phys. 122 084703 (2005).